Influence of Topography on the Propagation of Isolated Eddies

JOSSY P. JACOB AND ERIC P. CHASSIGNET

*Division of Meteorology and Physical Oceanography, Rosenstiel School of Marine and Atmospheric Science,
University of Miami, Miami, Florida*

WILLIAM K. DEWAR

Department of Oceanography, The Florida State University, Tallahassee, Florida

ABSTRACT

An analytical and numerical study of isolated coherent vortices and topography is presented. The motivation for this work comes from many observations of vortices influenced in trajectory, propagation, and decay by encounters with midocean ridges, seamounts, and bottom slopes. In particular, analytical predictions relevant to vortex propagation and evolution are compared with numerical results for lenses on bottom slopes and mixed barotropic–baroclinic eddies over a variety of topographies. The latter case includes examination of short-term and long-term behavior. Analytical theories are found to work well for the bottom lenses, and short-term behavior is captured well by a simple theory that emphasizes barotropic dynamics for mixed vortices. The exception for the latter case occurs for counterrotating eddies (i.e., eddies with opposing upper- and lower-layer swirl), for which the evolution is dominated by vortex instability. Long-term evolution has no comparable theory, and the various possibilities for vortex behavior are delineated by means of exploratory numerical work. A specific application to the case of North Brazil current rings, which are observed to move at anomalous rates, is presented.

1. Introduction

Rings that detach from intense western boundary currents represent one of the most energetic components of the mesoscale eddy field in the World Ocean. These rings (or isolated eddies), with a scale of a few hundred kilometers, transport large amounts of energy, heat, and salt across frontal zones that otherwise act as barriers to mixing between different water masses. The drift of these rings in the ocean is generally attributed to a combination of the latitudinal variation of the Coriolis parameter (planetary β effect) and the advection or steering by external influences such as the large-scale circulation, interaction with topography, and advection by other rings. The drift of isolated eddies on a β plane has been extensively investigated analytically (Flierl 1977; Nof 1981, 1983a; Cushman-Roisin et al. 1990), experimentally (Firing and Beardsley 1976), and numerically (McWilliams and Flierl 1979; Mied and Lindemann 1979; Smith and Reid 1982; Killworth 1983; Chassignet and Cushman-Roisin 1991; Chassignet et al. 1990; Chassignet 1992; Dewar and Gailliard 1994). In this study, we focus on the effect of topography on the

propagation of isolated eddies. In particular, we ask whether eddy baroclinicity and barotropicity affect eddy–topography interactions, how the β effect compares with the topographic effect, and what the influences of topographic orientation are.

a. Observational background

Oceanic eddies apparently possess strong barotropic components and deep flows (Schmitt and Olson 1985; Olson et al. 1985; Olson and Evans 1986; McCartney and Woodgate-Jones 1991) and, as a result, can interact strongly with the ocean bottom. Gulf Stream rings have been observed to pass over the New England seamounts and propagate onto the continental shelf/slope regions (Cheney and Richardson 1976). Brown et al. (1986), based on satellite observations, suggest that ring–shelf interaction is a significant factor influencing Gulf Stream ring evolution. As they cross the South Atlantic, Agulhas eddies meet the Walvis and Mid-Atlantic Ridges, which affect their propagation and decay (Byrne et al. 1995; van Ballegooyen et al. 1994; Clement and Gordon 1995).

Large anticyclonic rings are shed from the retroflecting North Brazil Current and interact with the coast of South America as they move in a northwest direction (Richardson et al. 1994; Fratantoni et al. 1995). "Med-

Corresponding author address: Dr. Eric P. Chassignet, RSMAS/MPO, University of Miami, 4600 Rickenbacker Causeway, Miami, FL 33149-1098.
E-mail: echassignet@rsmas.miami.edu

dies'' (anticyclonic Mediterranean outflow eddies) also interact with topography, perhaps fatally, as reported by Richardson et al. (1989). Deep ocean eddies have been identified (Armi and D'Asaro 1980; Houghton et al. 1982; Nof 1983b) in the abyssal Mid-Atlantic Bight and in the polar oceans (Aagaard and Malmberg 1978; Bruce 1995).

b. Modeling background

The dynamics of barotropic modons interacting with topography have been investigated numerically (Carnevale et al. 1988; Grimshaw et al. 1994) and in the laboratory (Carnevale et al. 1991). Nof (1983a) proposed an analytical model of eddy propagation on a slope. Experimental studies by Mory (1985), Mory et al. (1987), and Whitehead et al. (1990), however, have shown considerable scatter in vortex speed. Smith and O'Brien (1983) found that anticyclones and cyclones respond differently in a two-layer model to a topographic upslope to the west, with the response being controlled by dynamics in the lower layer. Kamenkovich et al. (1996), motivated by Agulhas eddy observations, suggested vortices exhibit a variety of behaviors when encountering the Mid-Atlantic Ridge, from slowing to stalling to enhanced decay. Simmons and Nof (2002) recently considered the interaction of reduced-gravity vortices with islands, working out the regimes in which islands induce irreversible eddy fission.

There is a fairly rich literature dealing with vortices and continental shelf or slope interactions. Shi and Nof (1993) argued for ''wodon'' behavior being a generalization of the modon solution of Stern (1975) to a case with vertical side walls. Dewar (2002) argued for the dominating effects of idealized, but realistic, lateral basin topography on the evolution of hetons. Sutryin (2001) has studied β-driven vortex encounters with weak slopes and emphasized the effects of topographic wave propagation on vortex evolution.

c. The present study

Much of our present analytical knowledge of ring evolution comes from studies in which the eddy is confined to an active layer (reduced gravity approximation), a problem that is analytically tractable (Nof 1983a,b; Cushman-Roisin et al. 1990; Chassignet and Cushman-Roisin 1991; Lebel 1994). Barotropic effects and baroclinic instabilities are excluded in this approach. The importance of the barotropic component on ring evolution was, however, recently emphasized by Dewar and Gailliard (1994) for a flat-bottom configuration. The barotropic component provides a mechanism by which an upper-layer eddy will be influenced by the topography.

In this paper, the interaction of eddies with topography is investigated in a hierarchy of models (analytical and numerical). We expand upon those studies discussed

above mostly by involving strong (as opposed to weak) interactions with topography. In section 2, we investigate, analytically and numerically, eddy–topography interaction in a reduced-gravity model in which the active layer is in direct contact with the bottom topography. The analytical predictions are compared in detail with results of a reduced-gravity numerical model. The impact of a barotropic component on the interaction of upper-layer eddies with topography is then analyzed, in section 3, using the approximate model proposed by Dewar and Gailliard (1994) modified to include topography. The validity regime of the approximate model results is evaluated against numerical simulations performed with a two-layer primitive equation model [Miami Isopycnic Coordinate Ocean Model (MICOM)]. These short (in time) experiments are complemented by long-term integrations of vortices interacting with a variety of topographies. The results define the influence of the topography on vortex propagation and dispersion. Last, in section 4, we consider an application to North Brazil Current rings. It has been suggested elsewhere that their propagation speeds are at odds with theory. We find good agreement with theory but note the extreme sensitivity of the formula to model parameters in the near-equatorial zone. The results are summarized and discussed in the concluding section.

2. Reduced-gravity model studies

We first derive an analytical solution for the translation speed of the center of mass for an eddy in the presence of generalized topography as in Cushman-Roisin et al. (1990), following Lebel (1994). The analytical model is then validated against a numerical reduced-gravity model.

a. Analytical model

The equations of motion for a one-and-one-half-layer, reduced-gravity system on a β plane after nondimensionalization by a length scale L, an interface displacement scale δH, and a timescale T are

$$\omega \mathbf{u}_t + \epsilon(\mathbf{u} \cdot \boldsymbol{\nabla})\mathbf{u} + (1 + \beta y)\mathbf{k} \times \mathbf{u} = -\boldsymbol{\nabla}\eta \quad (1)$$

and

$$\omega \eta_t + s\boldsymbol{\nabla} \cdot \mathbf{u} + \epsilon\boldsymbol{\nabla} \cdot (\mathbf{u}\eta) - \gamma\boldsymbol{\nabla} \cdot (\mathbf{u}b) = 0. \quad (2)$$

The nondimensional parameters are defined as

$$\omega = \frac{1}{f_o T}, \qquad \epsilon = \frac{g'\delta H}{f_o^2 L^2}, \qquad \beta = \frac{\beta_o L}{f_o},$$

$$s = \frac{g'H}{f_o^2 L^2}, \quad \text{and} \quad \gamma = \frac{g'b}{f_o^2 L^2},$$

where H is the undisturbed bottom-layer depth, η is the layer interface displacement, b is the topography, $\mathbf{u} = (u, v)$ are the zonal and meridional velocities, g' is the

reduced gravity, $\mathbf{k}$ is the unit vector in the z direction, and the Coriolis parameter f is defined as $f_o + \beta_o y$. The upper layer is motionless, and the layer thickness h is defined as $h = H + \eta - b$. In general, oceanic mesoscale eddies fall mostly into two categories, quasigeostrophic ($L \sim R_d$, $\delta H \ll H$; Kamenkovich et al. 1986) and frontal geostrophic ($L > 3R_d$, $\delta H \sim H$; Olson et al. 1985; Chassignet et al. 1990), where R_d is the Rossby radius of deformation. For an overview of the typical orders of magnitude of parameters found in oceanic mesoscale eddies, the reader is referred to Olson (1991).

The center of mass of an isolated eddy is defined by $X = \langle \eta x \rangle$ and $Y = \langle \eta y \rangle$, with $\langle \cdots \rangle = \iint \cdots \, dx \, dy / \iint \eta \, dx \, dy$ integrated over the domain. Integration of the continuity equation (2) over the domain and differentiation of X, Y with respect to time yield

$$\frac{d \iint \eta \, dx \, dy}{dt} = 0, \qquad C_z = \frac{dX}{dt} = \langle x \eta_t \rangle, \quad \text{and}$$

$$C_m = \frac{dY}{dt} = \langle y \eta_t \rangle, \tag{3}$$

where C_z and C_m are the zonal and meridional speed of the center of mass, respectively. Substituting η_t derived from (2) into (3), differentiating once again with respect to time (Ball 1963; Killworth 1983; Cushman-Roisin et al. 1990), and using (1) gives

$$\omega \frac{d^2 X}{dt^2} - \frac{dY}{dt} = \frac{s\beta}{\omega} \langle yv \rangle + \frac{\epsilon\beta}{\omega} \langle y\eta v \rangle - \frac{\beta\gamma}{\omega} \langle byv \rangle$$

$$- \frac{\gamma}{\omega} \langle b_x \eta \rangle \quad \text{and}$$

$$\omega \frac{d^2 Y}{dt^2} + \frac{dX}{dt} = -\frac{s\beta}{\omega} \langle yu \rangle - \frac{\epsilon\beta}{\omega} \langle y\eta u \rangle + \frac{\beta\gamma}{\omega} \langle byu \rangle$$

$$- \frac{\gamma}{\omega} \langle b_y \eta \rangle.$$

These equations can be simplified by considering that, to a first order, the velocities are in geostrophic balance because estimates of the Rossby number ϵ vary between 0.1 and 0.2 for anticyclonic rings and 0.1 and 0.4 for cyclonic rings (Olson 1991). The order of magnitude of the error δ on the velocities created by this approximation is given by max ($\omega, s, \epsilon, \gamma$). For vortices larger than the radius of deformation ($s < 1$), δ reduces to max (ϵ, β, γ) (Cushman-Roisin et al. 1990). This leads to

$$\omega \frac{d^2 X}{dt^2} - \frac{dY}{dt} = -\frac{\gamma}{\omega} \langle b_x \eta \rangle + \frac{\beta\gamma}{\omega} \langle b_x y\eta \rangle + O\left(\frac{s\beta\delta}{\omega}\right) \quad \text{and}$$

$$\omega \frac{d^2 Y}{dt^2} + \frac{dX}{dt} = -\frac{\gamma}{\omega} \langle b_y \eta \rangle + \frac{\beta\gamma}{\omega} \langle b_y y\eta \rangle + \frac{\beta\gamma}{\omega} \langle b\eta \rangle$$

$$- \frac{s\beta}{\omega} \langle \eta \rangle - \frac{\epsilon\beta}{2\omega} \langle \eta^2 \rangle + O\left(\frac{s\beta\delta}{\omega}\right).$$

Because ω is on the order of ϵ, the second-order terms $d^2 X/dt^2$ and $d^2 Y/dt^2$ can be neglected, and, after a conversion to dimensional quantities, we get, to first order, the analytic expression for the speed of the center of mass of an isolated eddy on a β plane with topography:

$$C_z = \underbrace{-\frac{g' \beta_o H}{f_o^2}}_{(a)} \underbrace{- \frac{g' \beta_o}{2f_o^2} \langle \eta^2 \rangle}_{(b)} \underbrace{- \frac{g'}{f_o} \langle \eta b_y \rangle}_{(c)}$$

$$+ \underbrace{\frac{g' \beta_o}{f_o^2} \langle \eta y b_y \rangle}_{(d)} + \underbrace{\frac{g' \beta_o}{f_o^2} \langle \eta b \rangle}_{(e)} \quad \text{and} \tag{4}$$

$$C_m = \underbrace{\frac{g'}{f_o} \langle \eta b_x \rangle}_{(f)} - \underbrace{\frac{g' \beta_o}{f_o^2} \langle \eta y b_x \rangle}_{(g)}, \tag{5}$$

where b_y and b_x are the meridional and zonal slope of the topography, respectively. The formal error for the zonal speed C_z is

$$\max\left(\frac{\beta_o g' H}{f_o^2}, \frac{g' b_y}{f_o}\right) \times \max\left(\delta, \frac{\omega^3}{s\beta}\right); \tag{6}$$

for the meridional speed C_m, it is

$$\frac{g' b_x}{f_o} \times \max\left(\delta, \frac{\omega^2}{s\beta}\right). \tag{7}$$

Term a is the long Rossby wave speed for the ambient fluid and is always westward. This is also the quasigeostrophic limit (McWilliams and Flierl 1979). Term b is the nonlinear contribution to the long Rossby wave speed due to the interface displacement. This term is negative for anticyclones ($\eta > 0$) and positive for cyclones ($\eta < 0$). Term c enhances or decreases the long Rossby wave speed, depending on the meridional slope of the topography. Term d reflects the interaction between β, the meridional slope of topography, and the interface displacement. Term e adjusts the long Rossby wave speed for the topography. Term f in the meridional speed analytic expression is equivalent to term c in the zonal speed expression. Term g in the meridional speed expression is equivalent to term d in the zonal speed expression.

For a flat bottom ($b = 0$), the analytical solution of Cushman-Roisin et al. (1990) is recovered. On an f plane ($\beta_o = 0$), the drift speed of the eddy depends only on the shape of the topography: $C_z = -(g'/f_o)\langle \eta b_y \rangle$, $C_m = (g'/f_o)\langle \eta b_x \rangle$. For a uniformly sloping topography (i.e., b_x and b_y are constant), the speed of propagation becomes independent of the eddy intensity, a result first derived by Nof (1983b).

TABLE 1. Eddy propagation speeds for the reduced-gravity numerical experiments. The initial interface displacement η_o is positive for anticyclonic eddies and negative for cyclonic eddies. The zonal (C_z) and meridional (C_m) propagation speeds are given for the eddy interface displacement maximum and for the center of mass at days 20 and 200, respectively.

| | | | | Interface max drift (cm s^{-1}) | | Center-of-mass drift (cm s^{-1}) | | | |
| | | | | | | Numerical | | Analytical | |
Expt	Plane	Slope	η_o (m)	C_z	C_m	C_z	C_m	C_z	C_m
RG1	f		300	−1.0/−1.8	−0.5/−0.2	−2.1/−1.8	0	−2.0	0
RG2	f		100	−1.0/−1.7	−0.2	−1.9	0	−2.0	0
RG3	f		−300	−0.9/−1.8	0.5/0.22	−1.8/−2.1	0	−2.0	0
RG4	β	S–N	300	−3.1/−5.1	−1.3/−0.5	−6.2/−4.6	−0.14	−5.4/−5.3	0
RG5	β	N–S	300	−1.2/−1.7	−0.2/−0.1	−2.1/−1.75	−0.01	−2.3/−2.2	0
RG6	β	E–W	300	−1.8/−3.5	−1.5/−2.2	−4.4/−3.9	−2.0	−4.0/−3.6	−1.7
RG7	β	W–E	300	−2.5/−3.5	−0.4/1.3	−4.1/3.14	1.7	−4.0	1.6
RG8	β	S–N	−300	−2.32/−4.4	1.4/0.7	−5.0/−5.7	0.1	−4.9/−5.0	0

b. Reduced-gravity numerical solutions

To discuss the validity of the analytical expressions (4) and (5), several numerical simulations were performed with a one-and-one-half-layer version of MI-COM (Bleck and Smith 1990; Bleck and Chassignet 1994). The model is configured in a domain of 2000 km × 2000 km with a uniform grid spacing of 20 km and with free-slip boundary conditions. The initial conditions consist of a Gaussian interface displacement profile:

$$\eta = \eta_o e^{-r^2/2R_{max}^2},$$

where r is the distance from the center of the eddy, η_o is the maximum interface displacement at the center of the eddy (usually 300 m), and R_{max} is the radius of the maximum velocity (taken to be 50 km). The velocity fields are initially in gradient balance, and the eddy is located far enough from the boundaries to be considered as isolated. The numerical dissipation is Laplacian with a coefficient $A_m = 200$ m^2 s^{-1}. The remaining param-

eters are chosen such that the Rossby radius of deformation R_d is equal to 45 km with H equal to 1000 m.

A series of experiments (Table 1) was first performed for a constant sloping topography slope of 10^{-4}. On an f plane, the center-of-mass propagation speed estimate is constant and is independent of the shape of the eddy according to (4) and (5). The first three experiments (RG1, RG2, and RG3), performed on an f plane ($\beta = 0$), correspond to two anticylonic eddies with $\eta_o = 300$ and 100 m, respectively, and to one cyclonic eddy with $\eta_o = 300$ m. Figure 1 shows the trajectory and drift speed of the center of mass and interface for the three cases. The trajectory of the center of mass is along the isobath with no downslope motion in all cases. The trajectory of the maximum displacement shows a small meridional drift, with the anticyclonic eddies moving toward deeper water and the cyclonic eddy moving toward shallower water, as a result of the interaction of the eddy core with the topographic Rossby wave wake. The average zonal drift of the center of mass in the
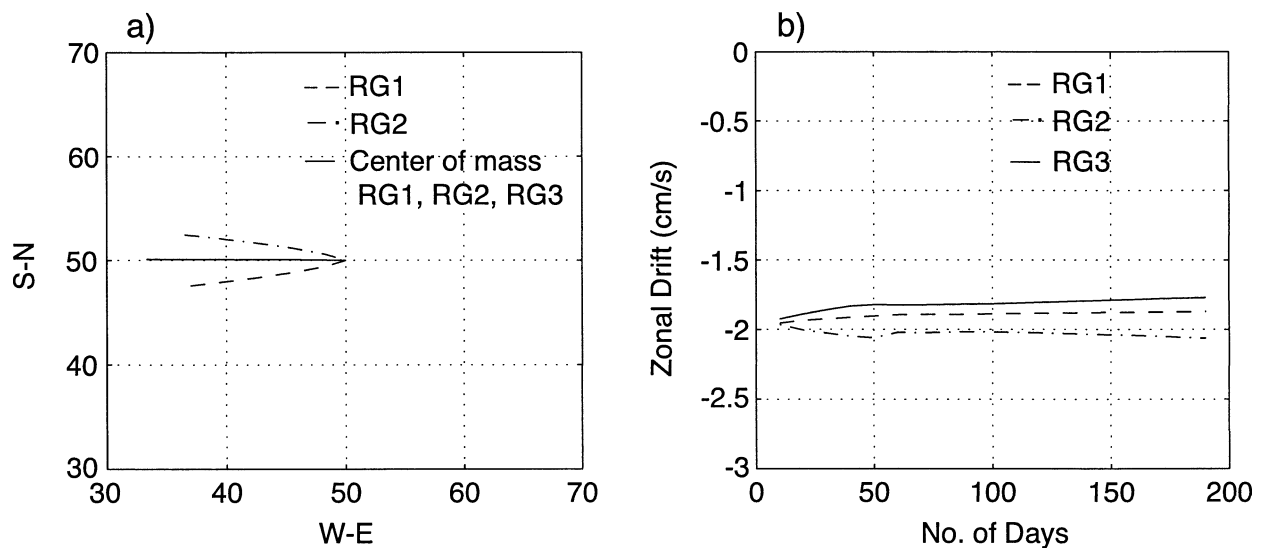

FIG. 1. Expts RG1, RG2, and RG3: (a) trajectory of the interface displacement maximum and of the center of mass and (b) zonal propagation speed of the center of mass.
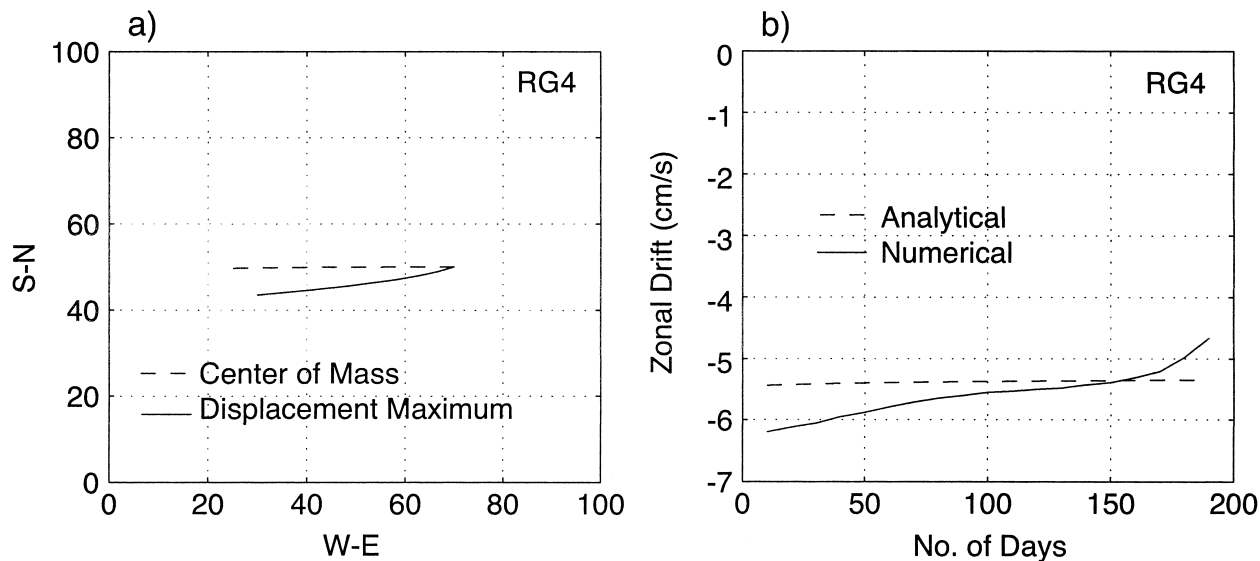
Fig. 2. Expt RG4: (a) trajectory of the interface displacement maximum and of the center of mass and (b) analytical and numerical zonal propagation speeds of the center of mass.

numerical experiments compares well with the analytical prediction, and the variations in speed among the three experiments do not exceed 10%.

The next four experiments (RG4, RG5, RG6, and RG7) were performed on a β plane for an anticyclone and four orientations of the topographic slope (90° rotation for each case) to illustrate the importance of the topographic β effect on the eddy relative to the planetary β-induced westward motion. The analytical model prediction for the speed of the center of mass at a given time t is obtained by using the numerical values of η in (4) and (5). The upper limit for the error estimates (6) and (7) is 24% ($\epsilon = 0.24$, $s = 0.8$, $\beta = 0.01$, $\gamma = 0.02$, $\omega = 0.192$).

In the case of a slope to the *north* (expt RG4; Fig. 2), both the planetary and topographic β effects are in the same direction (westward). Numerical and analytical estimates of the center-of-mass zonal drift for RG4, averaged over 200 days, are also in excellent agreement with the analytical prediction (Table 1). In examining the various components of the zonal drift in (4), one sees that the term a (background long Rossby wave speed), equal to -4 cm s^{-1}, and the term c (topographic β effect), equal to -2 cm s^{-1}, are the major contributing terms to the propagation speed and are independent of the interface displacement η. The other contributing terms are b (decreases as the interface decays), d, and e (constant because the center of mass moves along isobaths). The meridional drift of the center of mass is zero in agreement with (5) because the zonal slope b_x is equal to zero.

For an eddy interacting with a *southward*-sloping topography (expt RG5; Figs. 3,4), the topographic β effect will oppose the planetary β effect and the westward propagation of the eddy should be much slower than

for a flat-bottom case. For the chosen parameters, the center of mass propagation is to the west and, as in RG4, the terms a and c are the largest, but with opposite signs. An increase in the steepness of the slope increases the topographic β effect: the eddy stalls for a slope of 2×10^{-4} and moves eastward for a slope of 3×10^{-4} (Fig. 3).

For a uniformly increasing bottom topography to the *west* or to the *east* (expts RG6 and RG7; Fig. 4), the planetary and topographic effects are at a right angle. Again, there is a good agreement between the numerical and analytical predictions for the average center-of-mass propagation speeds.

The evolution of interface displacement contours after 100 and 200 days is shown for experiments RG5, RG6, and RG7 in Fig. 4. In a comparison of the interface displacement decay rate of the eddy for different topographic orientations, an eddy in the presence of northward-sloping topography undergoes a much larger decay than in the presence of a southward slope. This result is due to the fact that, in the presence of a northward slope, both the planetary β effect and the topographic β-like effect are in the same direction, therefore increasing both Rossby wave radiation and dispersion (Flierl 1984). When the eddy interacts with a southward-sloping topography, the two effects partially cancel each other, therefore causing less decay. A westward slope also causes more decay when compared with an eastward slope because, in the former, the eddy propagates to a shallower region, which results in stronger vortex stretching for an anticyclonic eddy.

Simulations for a cyclonic eddy (expt RG8, not illustrated) show that the center of the vortex propagates in the northwest direction (i.e., toward regions of higher topographic height), antisymmetric to the trajectory for
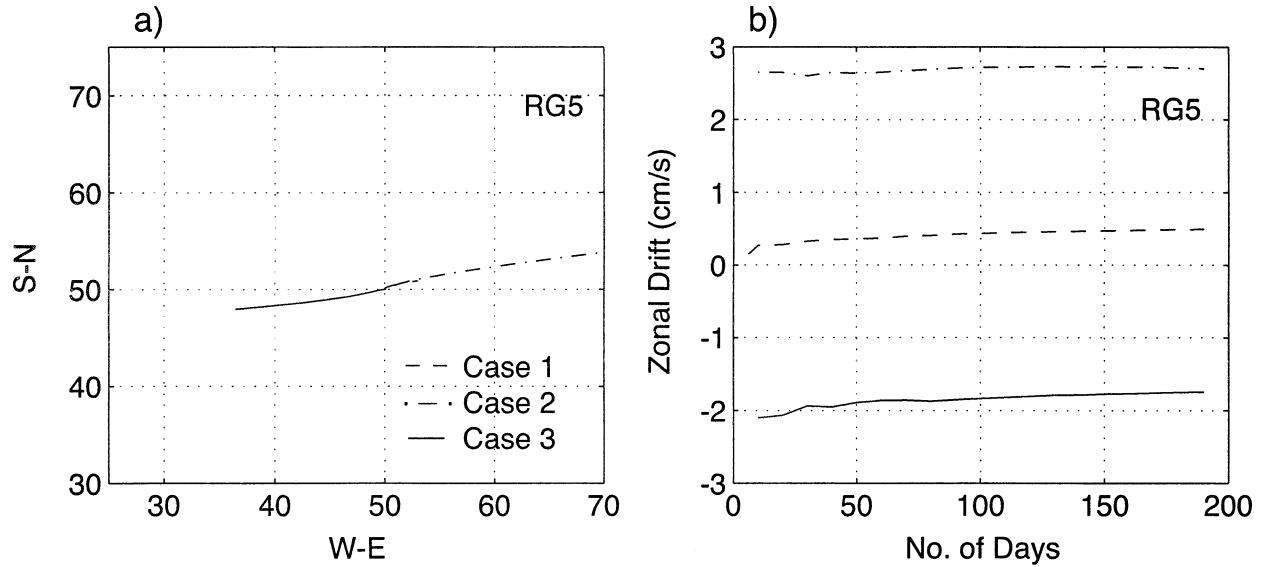
FIG. 3. (a) Trajectory of the interface displacement maximum and (b) zonal propagation speed of the center of mass for expt RG5 with three different slopes: case 1, slope $= 1 \times 10^{-4}$; case 2, slope $= 2 \times 10^{-4}$; case 3, slope $= 3 \times 10^{-4}$.

experiment RG4. The analytical speeds are in good agreement with the numerical values (Table 1).

In summary, good agreement ($\sim$5%–8%) is obtained between the numerical and analytical predictions for the center-of-mass displacement speeds. The analytical error estimate derived earlier from the analytical expressions (6) and (7) ($\sim$24%) is thus an upper bound. The differences between the analytical and numerical results are attributed to neglecting the second-order terms and using geostrophic velocities in the derivation of the analytical solution and to the dissipation present in the numerical model.

3. Importance of the barotropic component

Observations indicate that many eddies possess coherent deep flows (Olson et al. 1985; Olson and Evans 1986; Byrne et al. 1995), and we now consider their impact. Dewar and Gailliard (1994) studied eddies with strong deep flows in a flat-bottomed setting and demonstrated the role of the barotropic mode in controlling vortex propagation. This was accomplished by comparing an approximate model with primitive equation runs. In this section, the Dewar and Gailliard (1994) approximate model is modified to include topography and is used to investigate eddy–topography interaction.

a. Approximate model

Consider a two-layer β-plane system with a thermocline depression (or elevation) δh and topography b. Given our interest in lower-layer flows, the pressure gradients in both layers are scaled using the isopycnal depth variations, $p_i = g' \delta h$. This implies that the free surface scales as $\delta \eta = g' \delta h / g$. Assuming geostrophy

and $\delta h \sim H_1$, where H_1 is the far-field upper-layer thickness, the layer velocities scale as $U_i = f_o R_d^2 / L$, where L is the length scale of the eddy, and R_d is the Rossby deformation radius $g' H_1 / f_o^2$. The nondimensional equations of the two-layer system are

$$\omega \mathbf{u}_{1t} + \epsilon \mathbf{u}_1 \cdot \nabla \mathbf{u}_1 + (1 + \beta y)\mathbf{k} \times \mathbf{u}_1 = -\nabla \eta, \quad (8)$$

$$h_t + \nabla \cdot (\mathbf{u}_1 h) = 0, \quad (9)$$

$$\omega \mathbf{u}_{2t} + \epsilon \mathbf{u}_2 \cdot \nabla \mathbf{u}_2 + (1 + \beta y)\mathbf{k} \times \mathbf{u}_2 = -\nabla(\eta - h), \quad (10)$$

and

$$-\hat{\delta} h_t + \nabla \cdot [\mathbf{u}_2 (1 - \hat{\delta} h - \gamma b)] = 0, \quad (11)$$

where

$$\beta = \frac{\beta_o L}{f_o}, \qquad \epsilon = \frac{g' H_1}{f_o^2 L^2}, \qquad \hat{\delta} = \frac{H_1}{H},$$

$$\gamma = \frac{B}{H}, \quad \text{and} \quad \omega = \frac{1}{f_o T}.$$

Here, B denotes the maximum height of the topography, H is the total fluid thickness, and $\mathbf{u}_i = (u_i, v_i)$ are the layer-i velocities. These parameters measure the importance of β, inertia, the lower layer, and topography, respectively. Dewar and Gailliard (1994) selected the parameter ordering $1 \gg \epsilon \sim \omega \sim \hat{\delta} \geq \beta \geq \epsilon^2$ from an analysis of observations. We adopt this scaling here, along with the topographic scaling $H_1 \sim B$ or $\hat{\delta} \sim \gamma$. Geostrophy results at leading order in an ϵ-based expansion. Predictive equations are obtained at next order and are
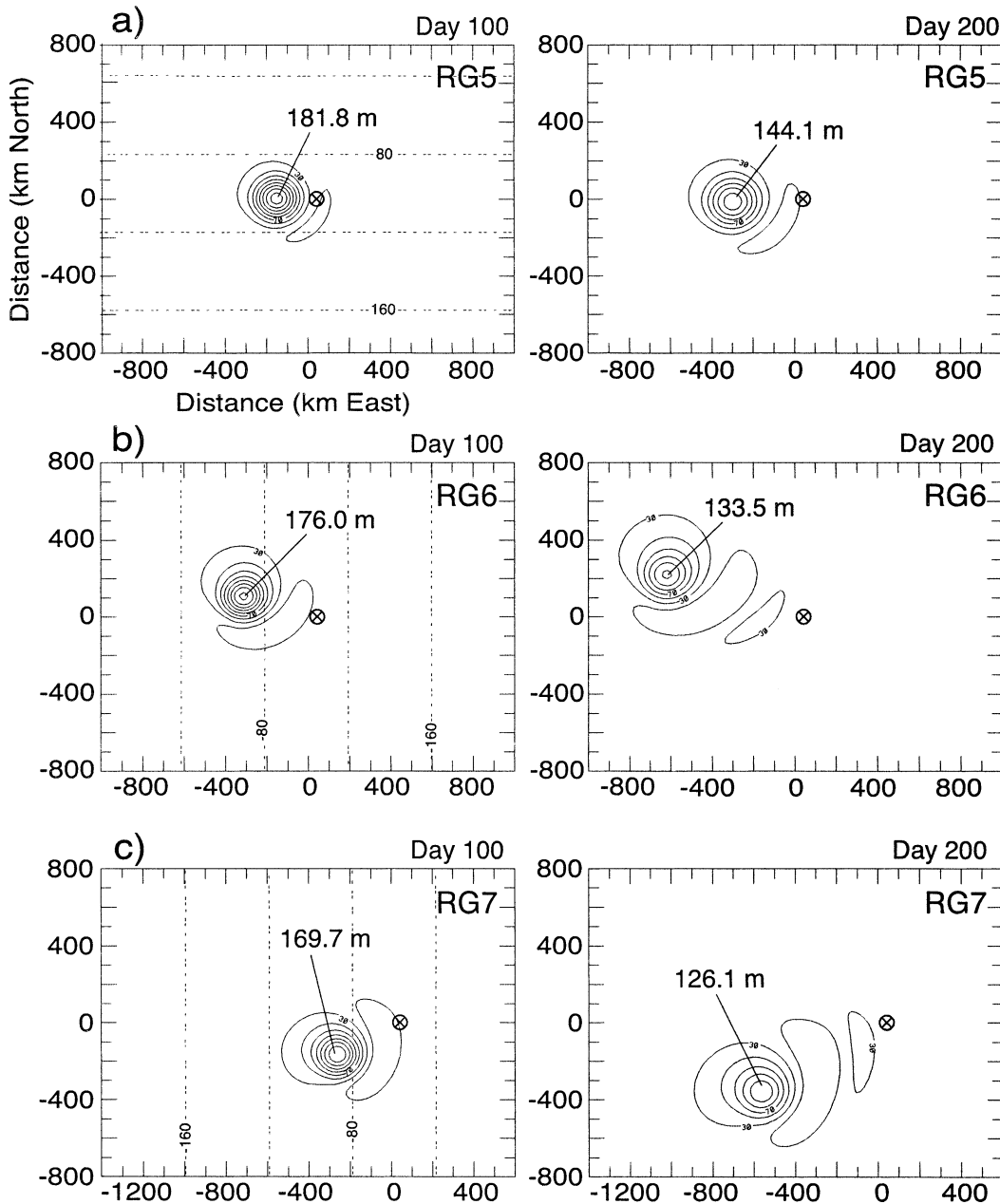
FIG. 4. Time evolution of the interface displacement contours (after 100 days and 200 days, respectively) for expts (a) RG5: southward slope, (b) RG6: eastward slope, and (c) RG7: westward slope. Topographic contours are plotted for $t = 100$ days, and the $\otimes$ is the position of the eddy at $t = 0$. The contour interval is 20 m.

$$h_t + J(\eta - h, h) = 0 \tag{12}$$

$$[\nabla^2(\eta - h)]_t + J\left[\eta - h, \nabla^2(\eta - h) + \frac{\beta}{\epsilon}y + \frac{\gamma}{\epsilon}b\right]$$
$$= 0, \tag{13}$$

where J denotes the usual Jacobian. Note that our assumption about the size of the topography brings in its effect at the same order as the other interesting dynamics in the model. The above is also expected to be valid for

timescales of order $T = O(\epsilon^{-1}f_o^{-1})$, which resembles a barotropic timescale. This is as opposed to more standard baroclinic theories with weak barotropic expressions, for which the limiting timescale is a baroclinic timescale of $O(\epsilon^{-1}T)$ (Cushman-Roisin et al. 1990).

Equation (13) constitutes one equation in the unknown $\eta - h$, the lower-layer pressure, and can be solved independently. The $(\eta - h)$ solutions can then be used to obtain η from (12). Topography is an additional effect in (13) when compared with the flat-

bottom case of Dewar and Gailliard (1994). Equation (13) is essentially a barotropic potential vorticity equation, and (12) argues that the upper-layer thickness is passively steered by lower-layer advection. Any nonpassive thickness evolution involves interface deformation and is too slow to produce sizeable changes in h on the rapid timescale of $O(T)$. We here solve (12) and (13) numerically and compare the solutions with those obtained from comparable two-layer MICOM experiments.

b. Configuration and initialization of the models

Both the approximate model and MICOM are configured in a two-layer 1280 km $\times$ 1280 km square domain on a β plane, with a grid spacing of 10 km and free-slip boundary conditions. A thickness diffusion K, taken as 100 m^2 s^{-1}, and a lateral viscosity coefficient A_m, set at 100 m^2 s^{-1}, are used in both models. The approximate model (AM hereinafter) requires them to be numerically stable. In AM, A_m is also a quadratically increasing function of position closer than 200 km to the boundaries. The time step for the approximate model is 1 h, and for MICOM the baroclinic time step is 450 s with a ratio of baroclinic to barotropic time step of 20.

The models are initialized with a radially symmetric Gaussian-shaped eddy profile at the free surface and at the interface:

$$\eta = \eta_o e^{-r^2/2R_{\max}^2}, \quad \delta h = h_o e^{-r^2/2R_{\max}^2},$$

where η_o, h_o are the maximum displacements of the free surface and of the interface, respectively, r is the distance from the center of the eddy, and $R_{\max}$ is the radius of maximum velocity. The lower-layer pressure P_2 is computed from the η and h profiles and is equal to $g\eta - g'h$.

The initial flow in the lower layer depends on the gradient of lower-layer pressure P_2. A parameter R, which relates the maximum interface displacement h_o and the maximum free-surface variation η_o, is introduced to control the lower-layer flow in the experiments. Parameter R is defined as

$$R = \frac{g\eta_o}{g'h_o} \begin{cases} > 1 & \text{barotropically dominated eddy} & \text{(a)} \\ = 1 & \text{compensated eddy} & \text{(b)} \\ < 1 & \text{counterrotating eddy} & \text{(c)} \end{cases}$$

Case a produces an eddy with the same sense of rotation in both layers, case b produces a compensated eddy with no flow in the lower layer, and case c produces an eddy with the flow in the lower layer opposite to that in the upper layer. In MICOM, the velocities in both layers are initialized using gradient balance for the chosen η and h fields.

TABLE 2. Short-term experiments using MICOM and the approximate model. The M experiments are performed with MICOM, and the AM experiments are performed with the approximate model. Parameter R defines the strength of the barotropic component (see text for details), and R_d is the Rossby radius of deformation (N indicates north).

Expt			R_d	Topographic	Eddy
AM	MICOM	R	(km)	slope	initialization
	M1	1.0	22	Flat bottom	Compensated
AM2	M2	1.5	22	Flat bottom	Corotating
AM3	M3	1.5	22	8×10^{-4} to N	Corotating
	M4	1.5	37	8×10^{-4} to N	Corotating
	M5	1.0	22	8×10^{-4} to N	Compensated
AM6	M6	1.5	22	16×10^{-4} to N	Corotating
AM7	M7	0.5	22	8×10^{-4} to N	Counterrotating

c. Short-term eddy-evolution experiments

Unless otherwise noted, the parameters used in these experiments are $g' = 0.98$ cm s^{-2}, $H_1 = 500$ m, $f_o = 10^{-4}$ s^{-1}, $\beta_o = 2 \times 10^{-11}$ m^{-1} s^{-1}, $h_o = 400$ m, $L = 50$ km, and the constant topographic slope is equal to 8×10^{-4}. With these values, $R_d = 22$ km, $\hat{\delta} = 0.125$, $\epsilon = 0.19$, and $\gamma = 0.25$. Experiments M1, M2, and AM2 are the flat-bottom reference experiments (see Table 2 for details).

1) BAROTROPICALLY DOMINATED ANTICYCLONIC EDDY ($R = 1.5$)

The 60-day evolution of the interface displacements for both experiments AM3 and M3 (approximately 12 times the theoretical time limit of validity for the approximate model) shows that the leading-order behavior of the models is comparable (Fig. 5). The interface decay of the eddy as well as its trajectory are quantitatively similar up to 30 days. After that, the approximate model differs from MICOM, yet the comparison is qualitatively favorable up to 60 days (see Fig. 6).

The approximate theory predicts that the upper-layer thickness h should be passively advected by the barotropic mode [cf. (12), (13)]. This is consistent with experiment M4 which is identical to M3, except for the layer thickness H_1, which is thicker (1400 m). The evolution of the interface displacement contours (Fig. 7) is similar to M3, with less dispersion, and is more stable. These results also show that the approximate theory gives reasonable results for relatively large δ and ϵ when compared with the primitive equation results and that the approximate theory is able to capture the leading-order behavior of eddy evolution for up to 60 days.

To investigate the robustness of the approximate theory, the sensitivity of the model to the size of the topography γ is investigated in AM6 and M6 in which a stronger bottom slope is used ($\gamma = 0.5$; Fig. 8). Again, the eddy evolution in both models is comparable up to 30 days. By day 60, however, the MICOM results show that the eddy becomes highly unstable and decays quick-
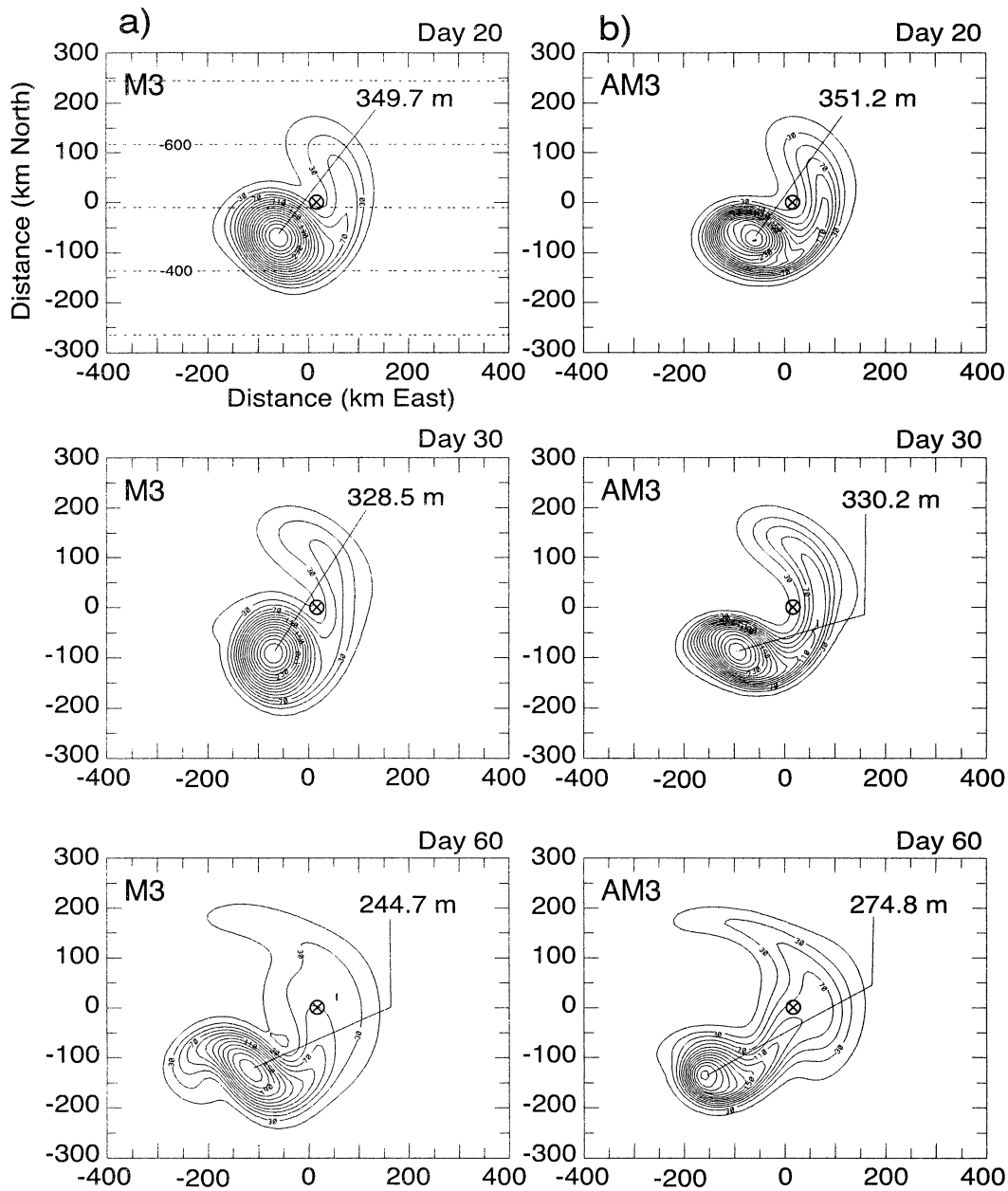
FIG. 5. Time evolution of the interface displacement contours for expts (a) M3 and (b) AM3. Topographic contours are plotted in the upper-left panel and the $\otimes$ is the position of the eddy at $t = 0$. The contour interval is 20 m.

ly, whereas the approximate model fails to represent these instabilities properly.

2) COMPENSATED ANTICYCLONIC EDDY ($R = 1.0$)

In the case of a compensated eddy, with the lower-layer flow initially set to zero, the approximate model's solution is trivial ($P_2 = g\eta - g'h = 0$, $h_t = 0$). The evolution of a compensated eddy is therefore shown only for a simulation with MICOM. In the presence of a northward uniform slope (M5), the interface displacement evolution (Fig. 9) shows that the propagation is

minimally influenced by the topography, and the evolution is very similar to that of a compensated eddy with flat bottom (M1). This result is in agreement with the work of Smith and O'Brien (1983) and Kamenkovich et al. (1996) and with observations (Clement and Gordon 1996; Byrne et al. 1995).

3) COUNTERROTATING ANTICYCLONIC EDDY ($R = 0.5$)

Experiments AM7 and M7 are performed with $R = 0.5$ for both MICOM and the approximate model. The
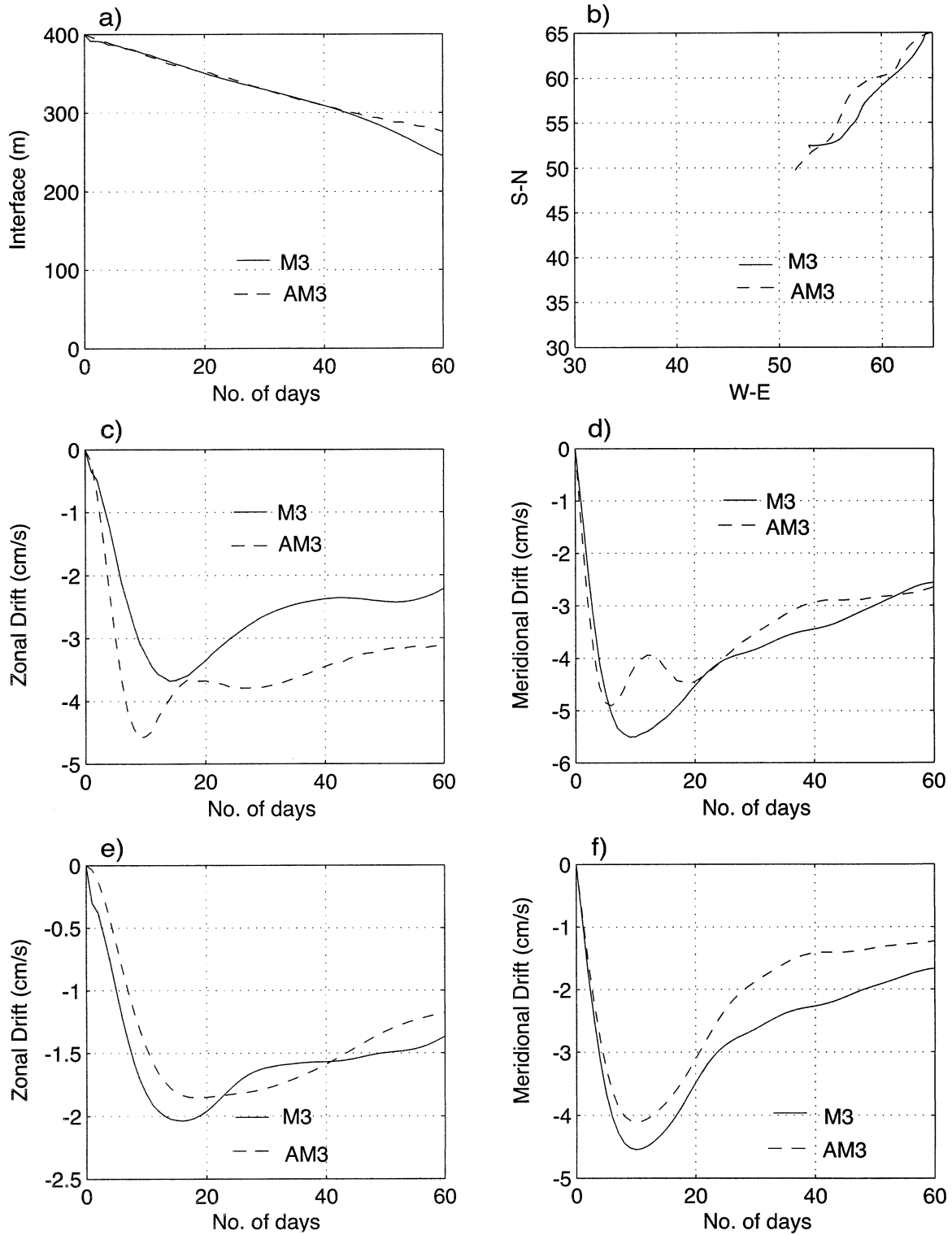
Fig. 6. Expts M3 and AM3: (a) eddy center interface decay, (b) trajectory, (c) zonal propagation speed of the interface displacement maximum, (d) meridional propagation speed of the interface displacement maximum, (e) center-of-mass zonal propagation speed, and (f) center-of-mass meridional propagation speed.
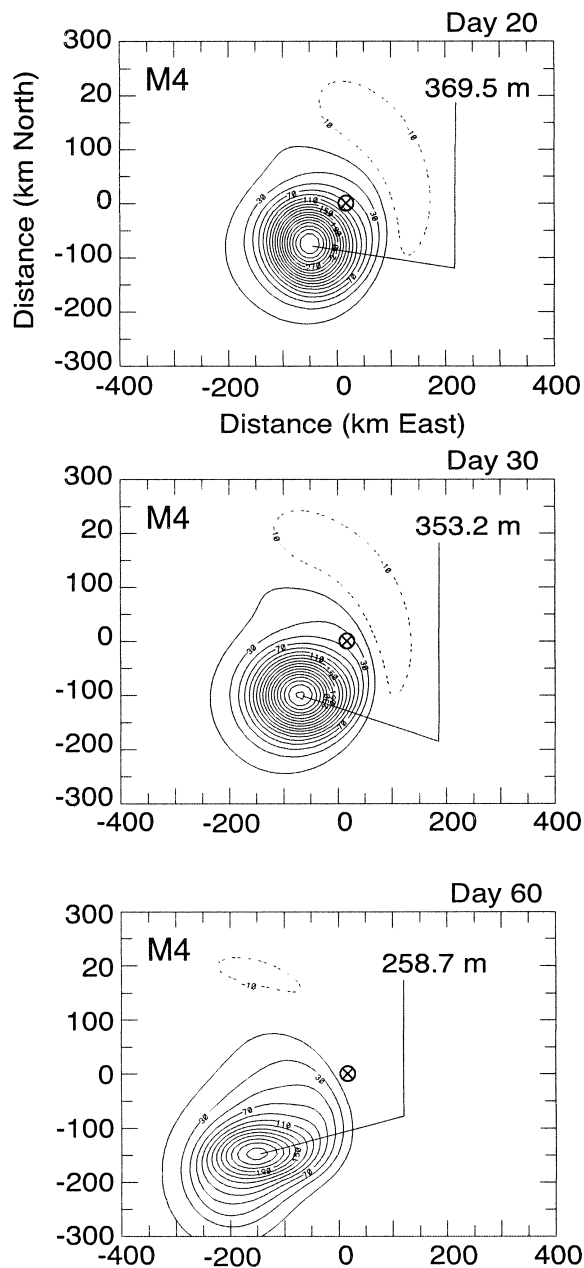
FIG. 7. As in Fig. 5 but for expt M4 (identical to M3, except that $H_1 = 1400$ m).

evolution of the interface displacement is shown in Fig. 10 for 60 days. In this case, the approximate model eddy evolution is significantly different from the MICOM results at 30 days. The eddy in M7 is highly unstable and becomes rapidly asymmetric; another center is formed by day 20, and the decay is rapid. Dewar and Killworth (1995) showed that counterrotating systems are generally unstable, and such dynamics are not represented in the approximate model.

In summary, topographic effects can be included in an approximate theory that emphasizes the dominance of the barotropic mode and its interactions with topography. Numerical experiments in the presence of topography for β-plane eddies, using MICOM and the approximate model, show that the approximate theory is accurate up to 60 days, as long as the eddy is corotating or compensated. Counterrotating eddies are found to be unstable, and the approximate theory is not applicable. The dynamics of the simplified theory are robust with respect to the sizes of ϵ, δ, and γ, reflecting the roles of inertia, layer thickness, and bottom height. Thus the evidence from these comparisons is that the leading-order dynamics of oceanic rings in the presence of topography are dominated by barotropic dynamics, at least for relatively short times. The principal effect is that a barotropically dominated eddy can be expected to move anomalously fast in both the zonal and meridional directions relative to a compensated eddy.

d. Long-term integrations with MICOM

In this section, we further investigate the importance of the barotropic component on the evolution of an anticyclonic eddy in the presence of topography for time periods longer than 30 days, the upper time limit of the approximate model's validity. Several long-term experiments ($\sim$200 days) were performed with the two-layer MICOM. A larger domain, 2000 km $\times$ 2000 km, is used for these longer time integrations so that the boundaries will not influence the eddy evolution. The eddy parameters used are $h_o = 300$ m, $g' = 1.6$ cm s^{-2}, $H_1 = 800$ m, $H = 4000$ m, $f_o = 1 \times 10^{-4}$ s^{-1}, $\beta_o = 2 \times 10^{-11}$ m^{-1} s^{-1}, $R_d = 36$ km, $R_{max} = 65$ km, and the topographic slope is equal to 8×10^{-4}. The list of experiments with the eddy initial conditions is given in Table 3. The trajectories of all eddies are displayed in Fig. 16.

1) NORTHWARD-SLOPING TOPOGRAPHY

To illustrate the relative impact of the topographic and planetary effects for eddies with and without a significant barotropic component ($R = 1.5$ and $R = 1$, respectively), we compare experiments with β only (no topographic effect; expts B1 and C1), with topography only (no planetary effect; expt B2), and with both effects (expts B3 and C3).

The center-of-mass drift speeds for B1, B2, and B3 are shown in Figs. 11 and 12. In the three cases, the eddy propagates southwestward with a stronger meridional (southward) than zonal (westward) translation because of the barotropic nature of the eddy [see previous section and Dewar and Gaillard (1994)]. The value of the topographic slope in B2 is equivalent to the strength of the planetary β effect in B1. The eddy propagation speeds are, however, smaller in B2 when compared with B1 because the planetary β effect influences the whole water column in B1, whereas in B2 the topographic β-like effect directly influences only the lower layer. In
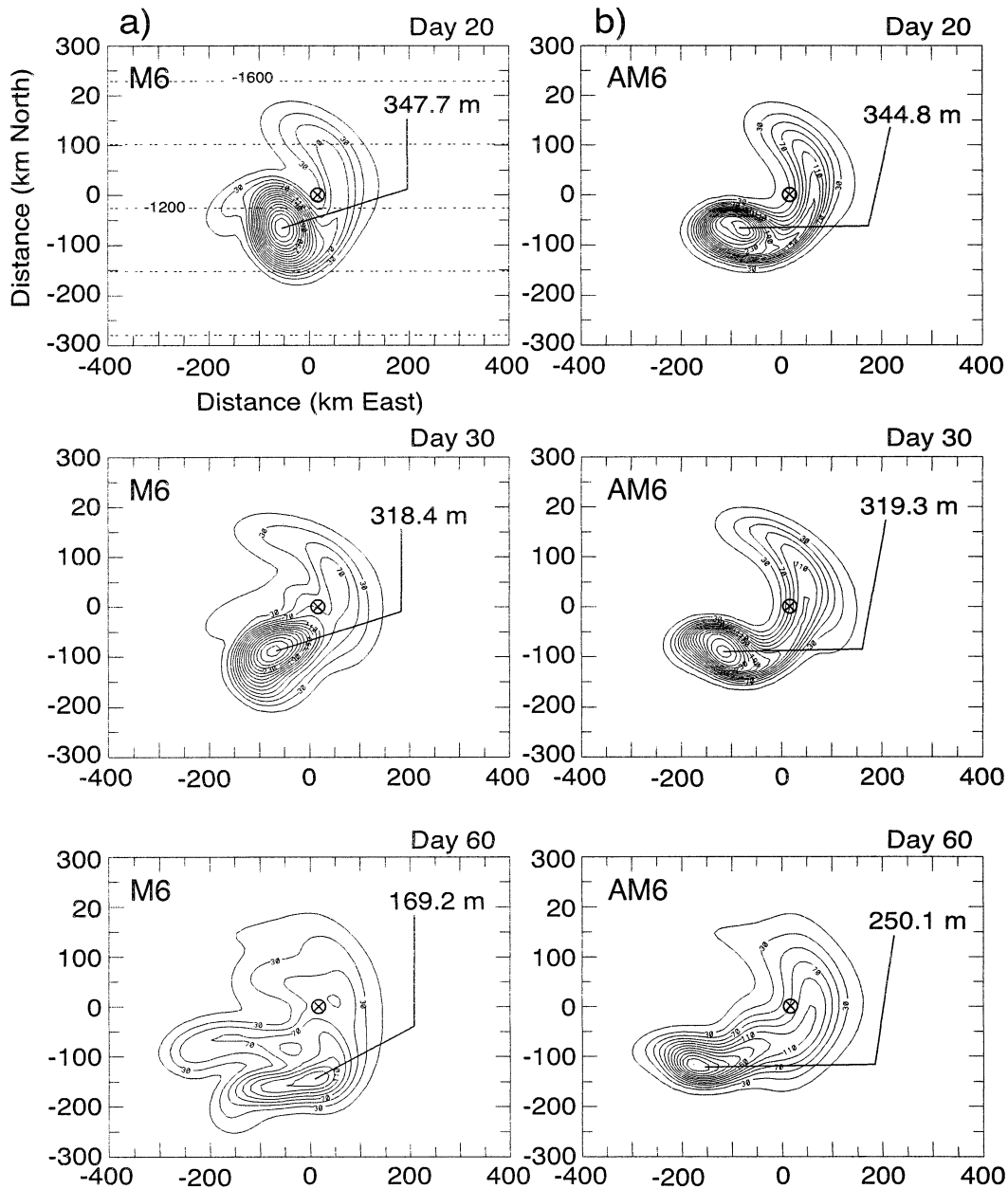
FIG. 8. As in Fig. 5 but for expts (a) M6 and (b) AM6.

the latter, the topography influences the upper layer indirectly via vortex stretching. In B3, the planetary and topographic effects act in the same direction and the translation speeds are larger in both the zonal and meridional directions when compared with either the flat-bottom (B1) or f-plane (B2) experiments. The Rossby wave radiation and associated dispersion are also stronger because of the combined planetary and topographic effects, and the eddy decays more rapidly.

Identical experiments C1 and C3, initialized with a compensated eddy and which differ from B1 and B3 only in their lower-layer flow, give eddy propagation

speeds that are much smaller, with a zonal propagation speed larger than the meridional speed (Fig. 12). In the barotropically dominated eddies B1, B2, and B3, the faster barotropic Rossby wave motion dominates. The eddy propagation speeds of the compensated eddies C1 and C3, however, become similar to the ones in B1 and B3 after 100 days. Although the lower layer is initially at rest for the compensated eddies, it is not constrained to stay motionless, and some motion in the lower layer is generated as the eddy propagates. After about 40 days, the eddies in C1 and C3 are no longer fully compensated (Fig. 17) and the barotropically dominated eddies B1
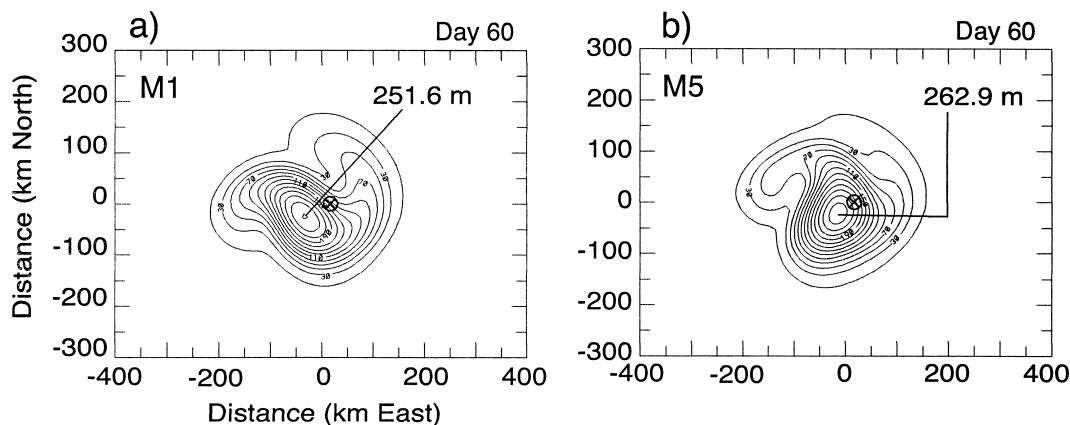
FIG. 9. Interface displacement contours after 60 days for expts (a) M1 and (b) M5. The $\otimes$ is the position of the eddy at $t = 0$, and the contour interval is 20 m.

and B3 reach a similar nearly compensated state (Fig. 17). The time evolution of the barotropic:baroclinic ratio R and the associated effect on the eddy propagation is summarized and discussed further in section 3d(4).

2) SOUTHWARD-SLOPING TOPOGRAPHY

When a southward slope is prescribed in B4, there is a considerable reduction in the eddy propagation speed when compared with that of B3 (Figs. 13 and 14). The eddy propagates mostly to the west with a small amount of meridional motion. In this experiment, the two effects (planetary and topographic) oppose each other. However, because the planetary effect acts over the whole fluid column, it is dominant, and the eddy moves primarily westward. The decay of the eddy in B4 (Fig. 13) is much slower when compared with that seen in B3, and the eddy retains its strength throughout the time period, even after 200 days. This result is mostly due to the cancellation of the two effects that leads to less Rossby wave dispersion and dissipation.

The compensated eddy in C4 behaves significantly differently from that in B4 and does not strongly feel the topography (Fig. 14). It propagates faster zonally and meridionally than in C3. In contrast to the other slope-orientation experiments, in which the eddies reach a nearly compensated state after 200 days (Fig. 17), the eddy in B4 retains its barotropically dominated state ($R \sim 1.5$), and the eddy in C4 reaches that state after 50 days (Fig. 17). This aspect is discussed further in section 3d(4).

3) WESTWARD- AND EASTWARD-SLOPING TOPOGRAPHY

In the presence of a westward or eastward slope, the planetary and topographic effects are orthogonal to each other. For a westward slope, the topographic effect has an eastward component and, in the case of the barotropically dominated eddy B5, cancels the planetary-induced westward motion (Fig. 15). As long as there is significant barotropic flow in the eddy, the topographic effect dominates and the trajectory (Fig. 16) shows the eddy propagating in a southeasterly direction. It then moves to the southwest. After about 50 days, the strong barotropic flow dissipates, the eddy reaches a compensated state (Fig. 17), and the eddy–topography interaction becomes minimal. The competition between the planetary and topography effects reduces the zonal speed considerably and results in the smearing of the vortex (Fig. 15). The compensated eddy (expt C5), on the other hand, propagates in a southwesterly direction (Fig. 16) with a propagation very similar to that seen in the flat-bottom case (expt C1) for up to 50 days, after which time the lower-layer flow becomes significant and starts to interact with the topography.

An eastward slope (expt B6) increases the westward drift of the eddy, and the overall propagation is southwest (Figs. 15 and 16). The eddy in B6 remains coherent for a longer period of time and propagates with less decay than in B5 (westward slope).

4) TIME EVOLUTION OF THE BAROTROPIC COMPONENT

The initial conditions are either a compensated state or a barotropically dominated one. However, as the eddy

TABLE 3. Long-term experiments using MICOM. The B series refers to the barotropically dominated eddies with $R = 1.5$, and the C series refers to the compensated eddies with $R = 1$. All experiments are on a β plane, except for B2, which is on an f plane.

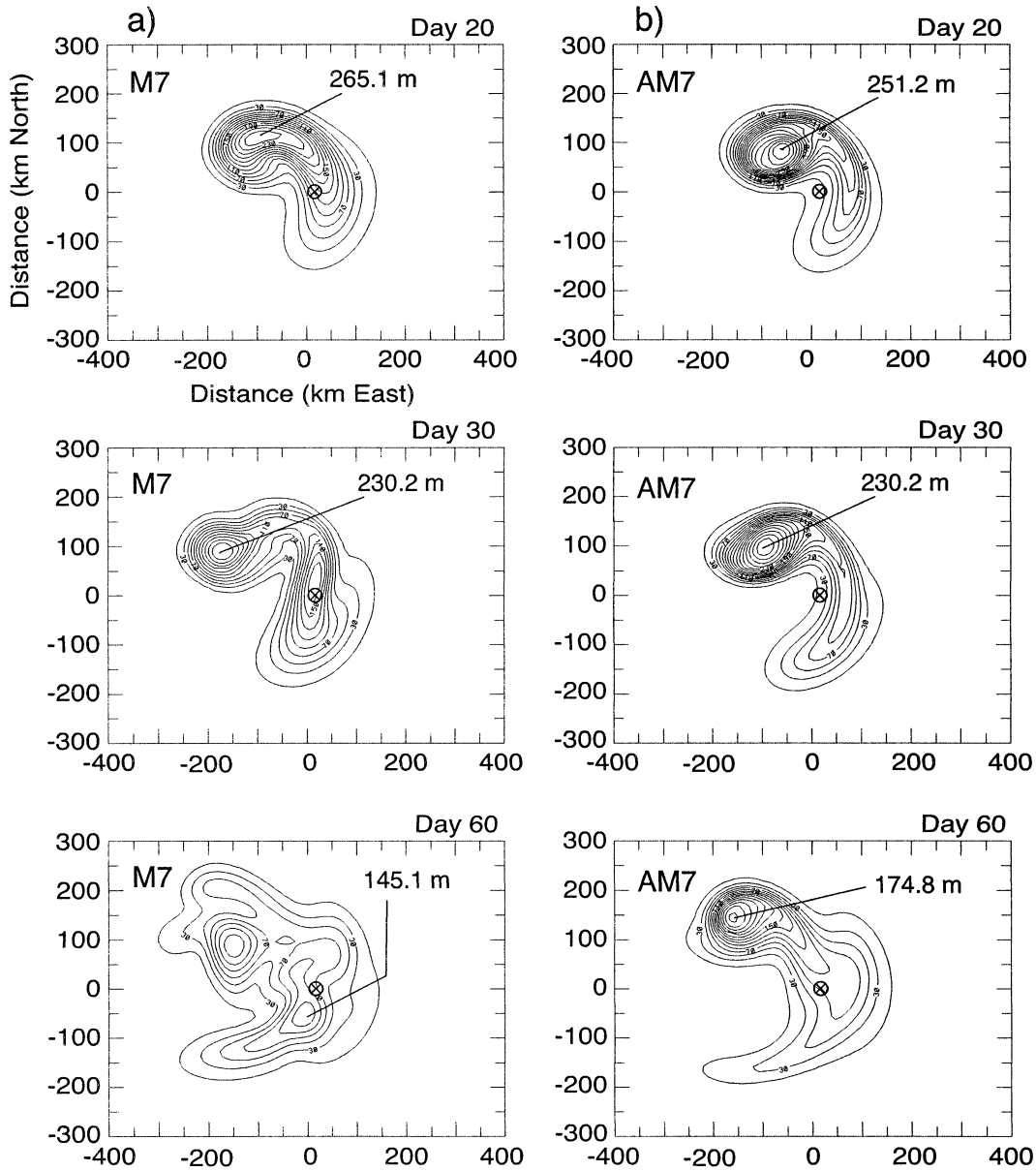| Expt		Characteristics
$R = 1.5$	$R = 1.0$	
B1	C1	Flat bottom
B2	—	f plane, northward slope
B3	C3	Northward slope
B4	C4	Southward slope
B5	C5	Westward slope
B6	C6	Eastward slope

FIG. 10. As in Fig. 5 but for expts (a) M7 and (b) AM7.

propagates, that initial state is not necessarily retained. To keep track of the evolution of the barotropic component during the 200-day time period, the parameter R was computed as a function of time from the sea surface height extremum and interface displacement extremum. It is plotted in Fig. 17 for all experiments listed in Table 3. Most of the eddies initialized with significant barotropic flow ($R = 1.5$) reach a nearly compensated structure (i.e., the barotropic component of the eddy decays as the lower-layer flow weakens) in about 40–50 days. Eddies initialized with a compensated lower layer approximately maintain that state ($R \sim 1$), although there is some lower-layer flow generated as the eddy evolves, modifying the eddy propagation.

There is one exception, the southward-sloping-topography experiments B4 and C4, in which the eddy either retains or reaches a barotropically dominated state ($R \sim 1.5$) after 200 days. The topographic slope-induced effect in these two experiments exactly cancels the planetary β effect in the lower layer. To analyze further the relative strengths of these two effects and shed some light on the different behavior of B4 and C4, four additional experiments were conducted with a southward slope (i) one-half of the original value (planetary effect stronger than topographic effect) and (ii) 2 times the original value (topographic effect stronger than planetary effect). The time evolution of R for these four additional experiments, as well as the interface displace-
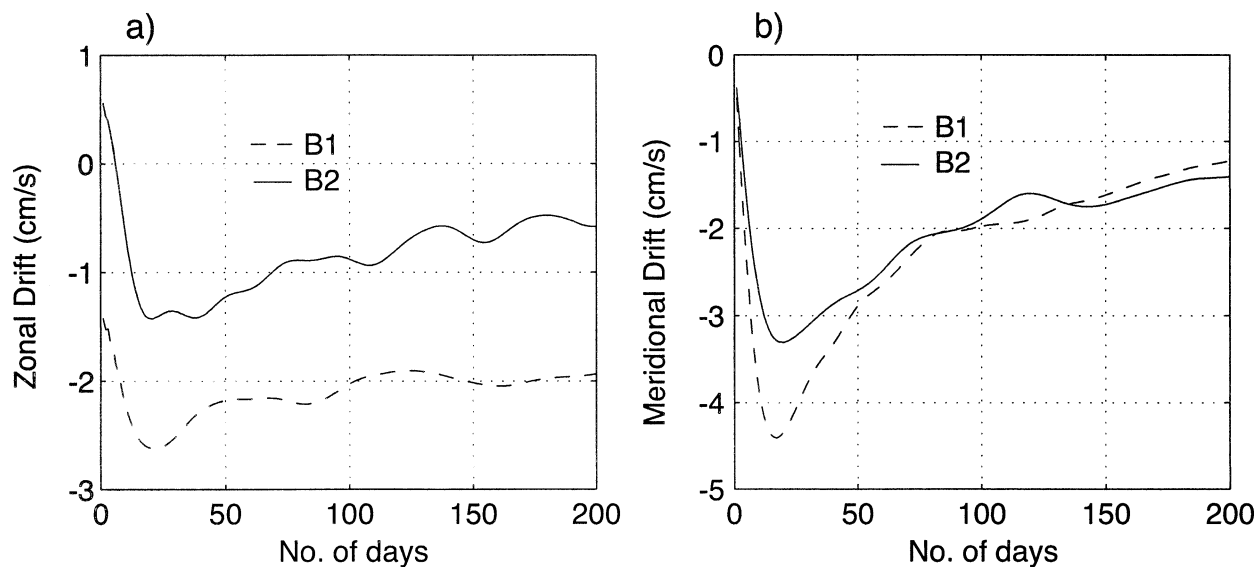
FIG. 11. (a) Zonal and (b) meridional propagation speeds of the center of mass for expts B1 and B2.

ment at day 120 for the barotropically dominated eddies ($R = 1.5$), is shown in Fig. 18. As expected, the direction of eddy propagation depends on the dominant effect, planetary or topographic.

When the topographic effect is not equal to the planetary effect, the time evolution of the ratio R (Fig. 18) shows that the barotropically dominated eddies ($R = 1.5$) evolve toward a compensated state after 100 days and that the compensated eddies ($R = 1$) mostly retain their original compensated state. These results, as well as the slow eddy decay seen in B4 and C4, indicate that when there are weak Rossby wave radiation and dispersion (opposite topographic and planetary effects), the decay of the eddy as well as the decay of the barotropic

component is slow. When either effect (planetary or topographic) is allowed to dominate, there is more barotropic Rossby wave dispersion and the eddy becomes compensated.

4. Idealized simulations of North Brazil Current ring interactions with topography

Fratantoni et al. (1995) report that the observed North Brazil Current (NBC) rings propagate at a much slower rate than that predicted by the analytical theories of Cushman-Roisin et al. (1990) and Nof (1981). In contrast to the equatorward (southwestward) propagation of anticyclonic eddies in the Northern Hemisphere,
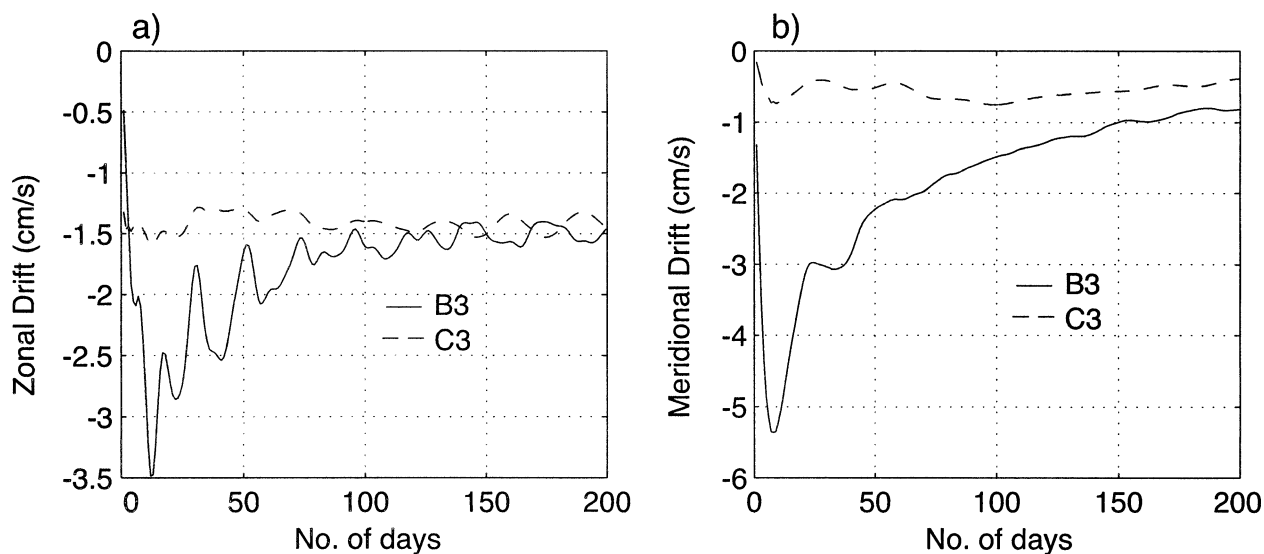
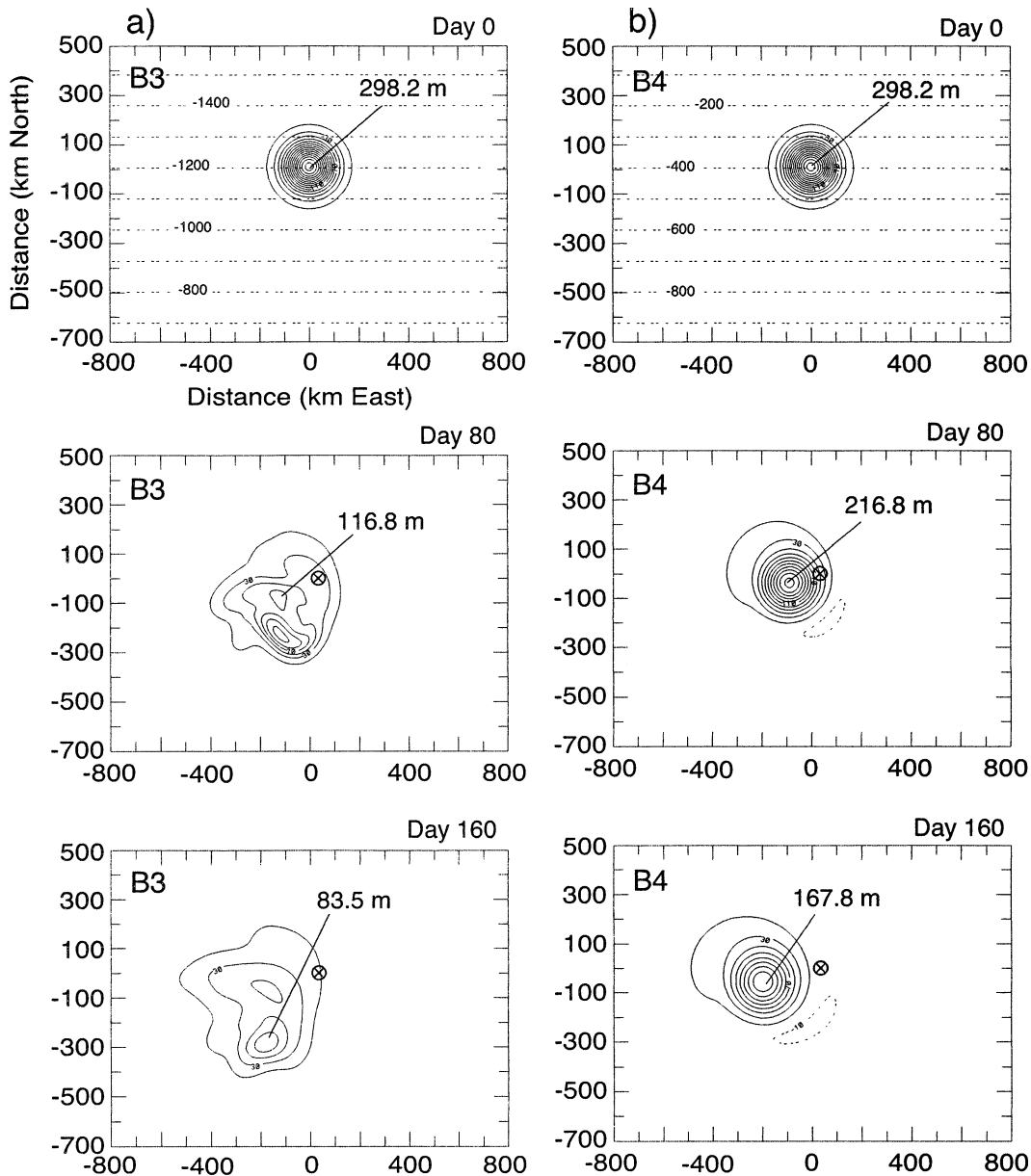

FIG. 12. As in Fig. 11 but for expts B3 and C3.

FIG. 13. As in Fig. 5 but for expts (a) B3 and (b) B4.

these rings propagate poleward (northwestward) along the coast of South America. Interaction with the coastal shelf has often been suggested as a probable cause for their unusual northwest propagation (Nof and Pichevin 1996). In this section, idealized NBC ring experiments, performed with MICOM as configured in the previous section, are presented to evaluate the possible influence of the coastal shelf and topography on the rings' propagation.

The NBC rings are large anticyclonic eddies that are shed from the retroflecting North Brazil Current, between latitudes 7° and 10°N in the tropical western Atlantic (Johns et al. 1990). The lifetime of these rings is relatively short (~100 days). Because of the significant

variation of the Coriolis parameter in the equatorial region, these rings are very different from the midlatitude rings investigated in the previous sections. Based on Fratantoni et al. (1995) and on recent observations by W. E. Johns (2000, personal communication), the following parameters were chosen: $f_o = 0.2 \times 10^{-4}$ (8°N latitude), $\beta_o = 2.25 \times 10^{-11}$ m^{-1} s^{-1}, $H_1 = 300$ m, $H = 4000$ m, $h_o = 100$ m, $g' = 1.5$ cm s^{-2}, and $R_{\max} = 100$ km. Because most of the NBC rings have a significant barotropic component (Fratantoni et al. 1995), the numerical experiments were performed for $R = 1.5$ (barotropically dominated eddy).

Experiment NBC1 is a flat-bottom control experiment (not illustrated). The eddy interface displacement max-
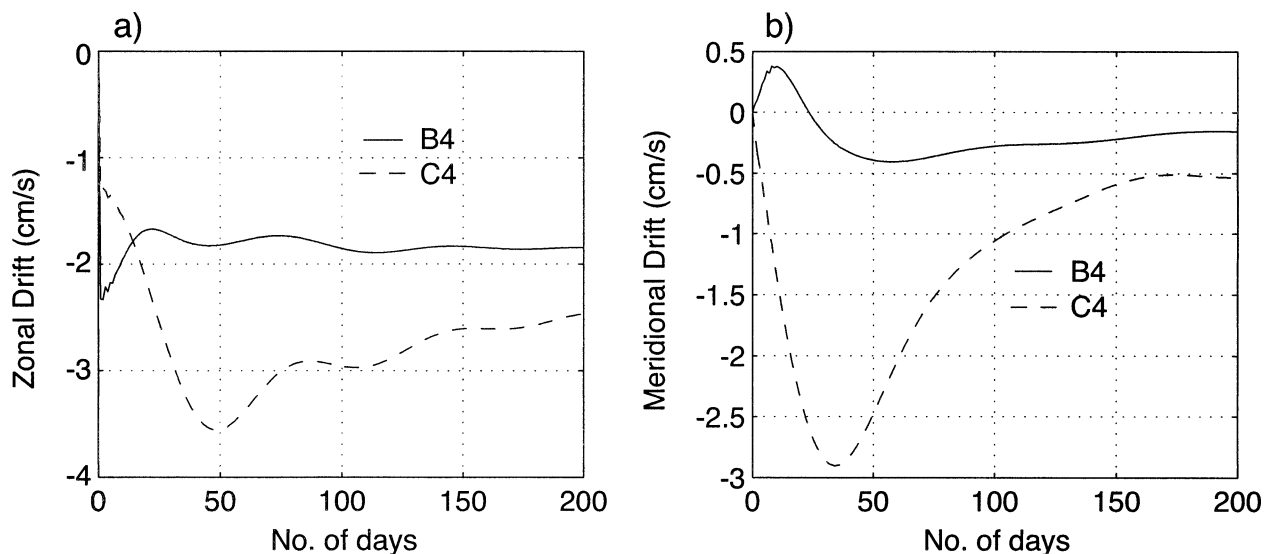
FIG. 14. As in Fig. 11 but for expts B4 and C4.

imum propagates westward at 11.7 cm s^{-1} and southward at 5.0 cm s^{-1}. These speeds are much larger than the typical translation speeds of midlatitude eddies because of the small Coriolis parameter f_o ($\sim$5 times smaller than at midlatitudes). Note that the meridional propagation does not dominate the westward motion when significant barotropic flow is present in the eddy, in contrast to the previous results. This is due to the small interface displacement combined with the large eddy radius and small background upper-layer thickness. An identical experiment performed with $R = 1$ (compensated eddy) confirmed that the barotropic component has only a small impact for the above ring parameters. The eddy decays relatively fast, and the eddy propagation is influenced by the boundaries after 60 days.

As the NBC rings move along the northeast coast of South America, they encounter topography in the form of a continental slope. The bathymetry in the NBC region shallows from 4000 to 500 m in about 300–400 km. To simulate the NBC ring evolution for a quasi-realistic topography, a steep topographic slope oriented in the southwest–northeast direction was chosen. In experiment NBC2 (not illustrated), an intensification of the eddy's strength is observed as it reaches shallower depths after 20 days. The eddy propagates predominantly westward with a smaller southward motion. The zonal and meridional speeds of the eddy interface displacement maximum are 11.27 cm s^{-1} westward and 4.2 cm s^{-1} southward, respectively.

In summary, the eddy propagation speeds with and without topography do not differ much. When the eddy approaches steep topography, it intensifies and decays rapidly as it moves on the slope. The observed westward propagation speeds of the NBC rings are between 8 and 16 cm s^{-1} (Fratantoni et al. 1995), in agreement with

the model's predictions. The propagation speed of the center of mass ($\sim$18 cm s^{-1}) also agrees well with the Cushman-Roisin et al. (1990) analytical prediction of 19 cm s^{-1}. There is no northward component in the numerical experiments. This absence can be attributed to the fact that (i) the topography in the model does not extend above 500 m or include a coastline; (ii) influences from the large-scale steering flow are not considered; and (iii), unlike in midlatitude regions, large changes in the Coriolis parameter are encountered within short meridional distances over which the β-plane approximation may no longer be suitable. The importance of these factors on the NBC rings' propagation will be the focus of a separate investigation.

The choice of Coriolis parameter is extremely important in the case of NBC ring simulation. Fratantoni et al. (1995) reported that the NBC rings are much slower than the analytical predictions of Cushman-Roisin et al. (1990). At these low latitudes, a change in f value by only 1° of latitude can lead to a large change in the predicted propagation speed because of the f^2 term in the denominator of the analytical expression. In addition, the analytical prediction depends greatly upon the reduced gravity parameter chosen. In their analysis, Fratantoni et al. (1995) chose the Coriolis parameter for 7°N latitude and a larger reduced-gravity parameter (2.3 cm s^{-2}), leading to larger estimates of the analytical speeds (26–34 cm s^{-1}) for NBC rings. In the above experiments, we have chosen a Coriolis parameter corresponding to 8°N latitude, which is closer to the point where NBC rings actually separate from the North Brazil Current and begin to move independently. We have also used a reduced-gravity parameter (1.5 cm s^{-2}) that best matches the observed stratification in the region of our model configuration (W. R. Johns 2000, personal communication). For these parameters, the analytical
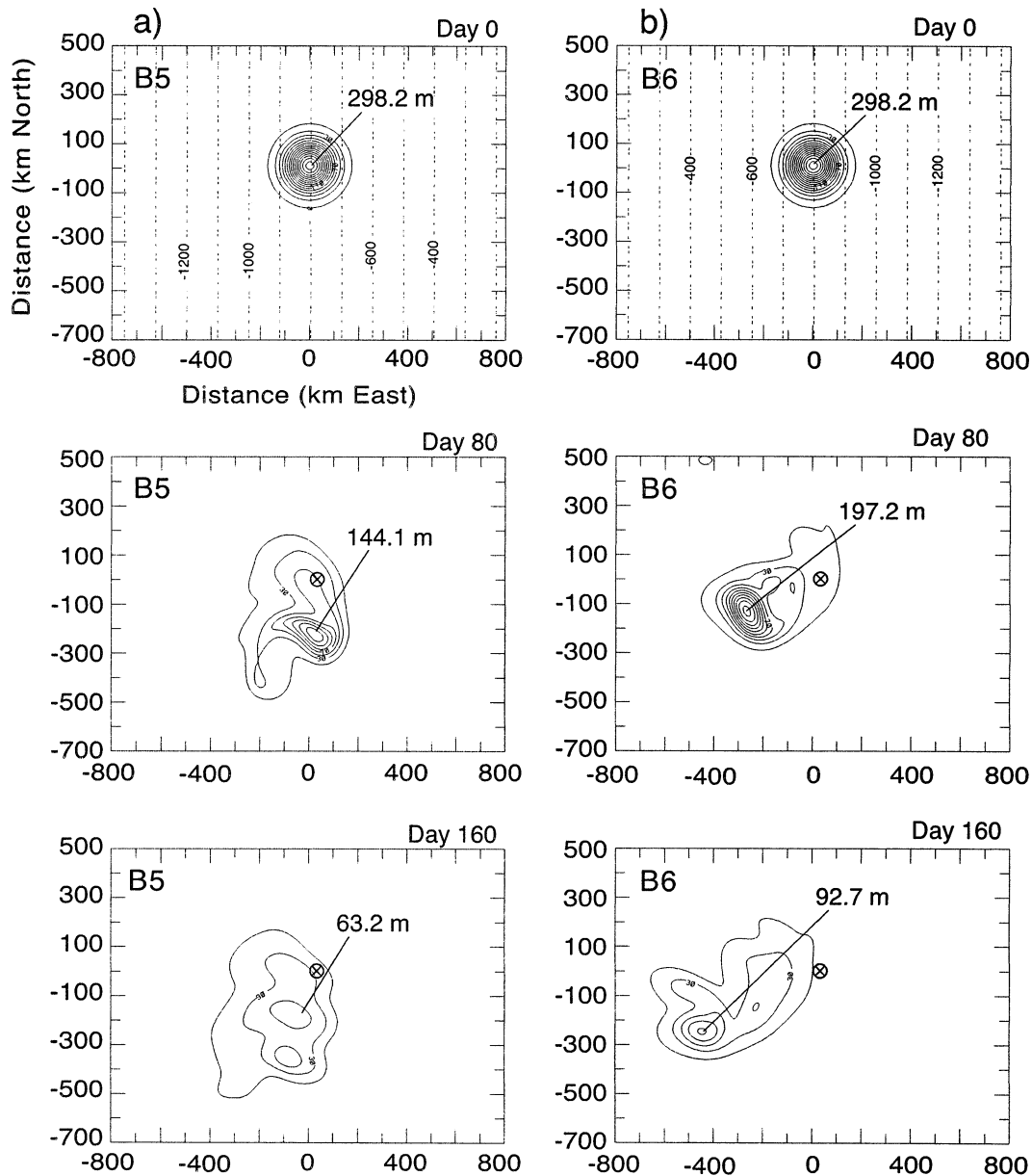
FIG. 15. Same as Fig. 5 but for expts B5 and B6.

speed estimates of Cushman-Rosin et al. (1990) agree with the observed speeds as well as with the model predictions.

5. Summary and discussion

The relative importance of the planetary β effect versus topographic effects, and the influence of barotropic flow in the presence of topography on the propagation and evolution of isolated eddies, have been investigated analytically and numerically. To understand and isolate the importance of the different mechanisms involved, a hierarchy of models with increasing complexity was used to simulate eddy–topography interaction.

The influence of topography on eddy propagation was first investigated analytically using the reduced-gravity approximation. Analytical solutions for the zonal and meridional translation speeds of the eddy center of mass were obtained, given the assumption that the eddy is in geostrophic balance and the neglect of higher-order terms for simplicity. To validate the analytical model predictions, a reduced-gravity numerical model was used, because such a model does not require the simplifying assumptions. Results indicate that the differences ($\leq 10\%$) in translation speed are within the theoretical error estimates of the analytical model assumptions.

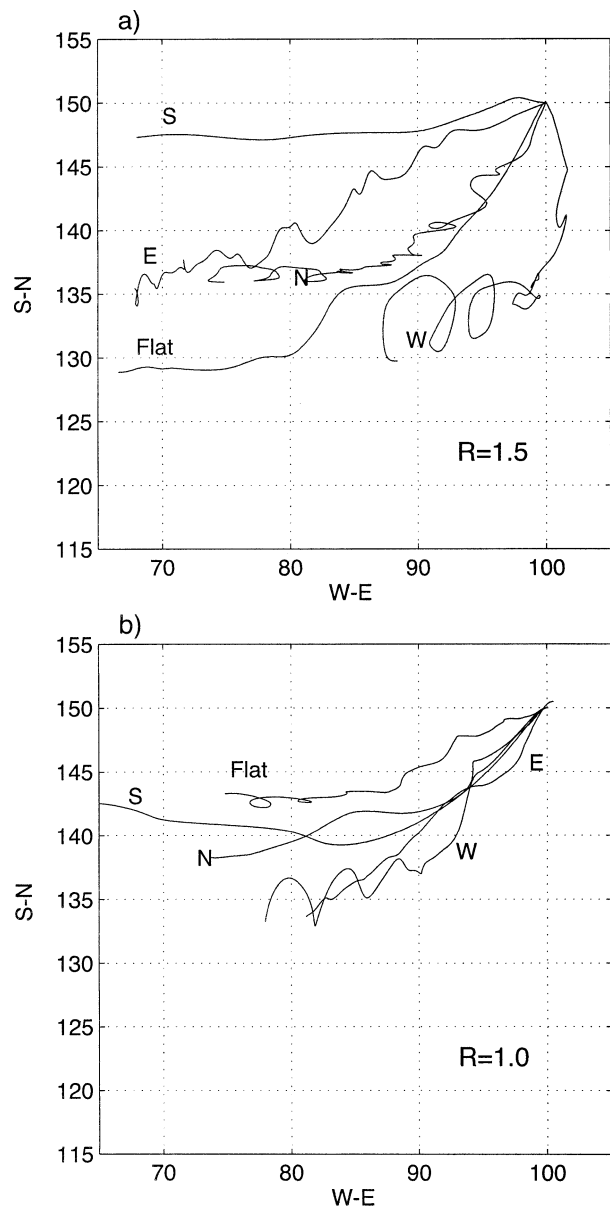The importance of barotropic flow in eddies in the

FIG. 16. Trajectories of the center of mass for expts (a) B1 (flat bottom), B3 (N: northward slope), B4 (S: southward slope), B5 (W: westward slope), and B6 (E: eastward slope) and for expts (b) C1 (flat bottom), C3 (N), C4 (S), C5 (W), and C6 (E).

using parameters beyond the legitimate range. The comparisons indicate that the theory is robust well beyond its limits. Results both from approximate and from MICOM experiments initialized with a barotropically dominated eddy indicate that vortex propagation increases significantly in comparison with a compensated eddy. This increased speed is due to a combination of slow baroclinic and fast barotropic Rossby waves. Meridional propagation can dominate, in contrast to the essentially westward propagation of reduced-gravity eddies. In a similar way, the topographic β-like effect also includes contributions from baroclinic and barotropic topographic Rossby waves, and the downslope component can dominate along slope drift.

The topographically steered flow modifies the planetary β-induced eddy propagation. The orientation and magnitude of the topographic slope determine the topographic influence, as expected from potential vorticity conservation of the system. However, eddies with flow penetrating to the bottom feel only the bottom topography, whereas compensated eddies do not. Hence, in addition to the orientation and magnitude of the topographic slope, eddy propagation in the presence of topography also strongly depends on the barotropicity of the eddy. The combined influence of β and topography modifies vortex propagation depending on their relative strength and orientation. Thus a northward-sloping topography increases the speed because both effects are in the same direction, whereas a southward slope decreases the propagation speed.

Eddy decay is mainly due to planetary wave dispersion. Although barotropically dominated eddies are more stable and robust configurations than are eddies with a compensated lower layer, their decay rate changes with topography. For a northward-sloping topography, because of the faster Rossby wave radiation and dispersion the eddy decays quickly, whereas in the presence of a southward-sloping topography the planetary and topographic effects partially cancel each other and hence the eddy dissipates slowly.

Eddy evolution for time periods longer than the upper limit of the approximate model validity (~30 days) was studied using MICOM. The long-term integrations indicate that the eddies with initial barotropic flow exhibit a tendency to reach a state of "deep compensation" (or the barotropic flow is no longer coherent with the eddy), as seen in previous studies with flat bottom (Mied and Lindemann 1979; McWilliams and Flierl 1979). Although the lower-layer flow appears to be nearly compensated after ~40–50 days, the presence of a significant barotropic component modifies the flow in both layers and thus affects further evolution and propagation. Eddies initialized with a compensated lower layer generate some lower-layer flow as they evolve, but the flow is not coherent with the upper-layer eddy. However, in the presence of southward-sloping topography, when both the planetary and topographic effects equally cancel each other, the eddy maintains the coherent baro-
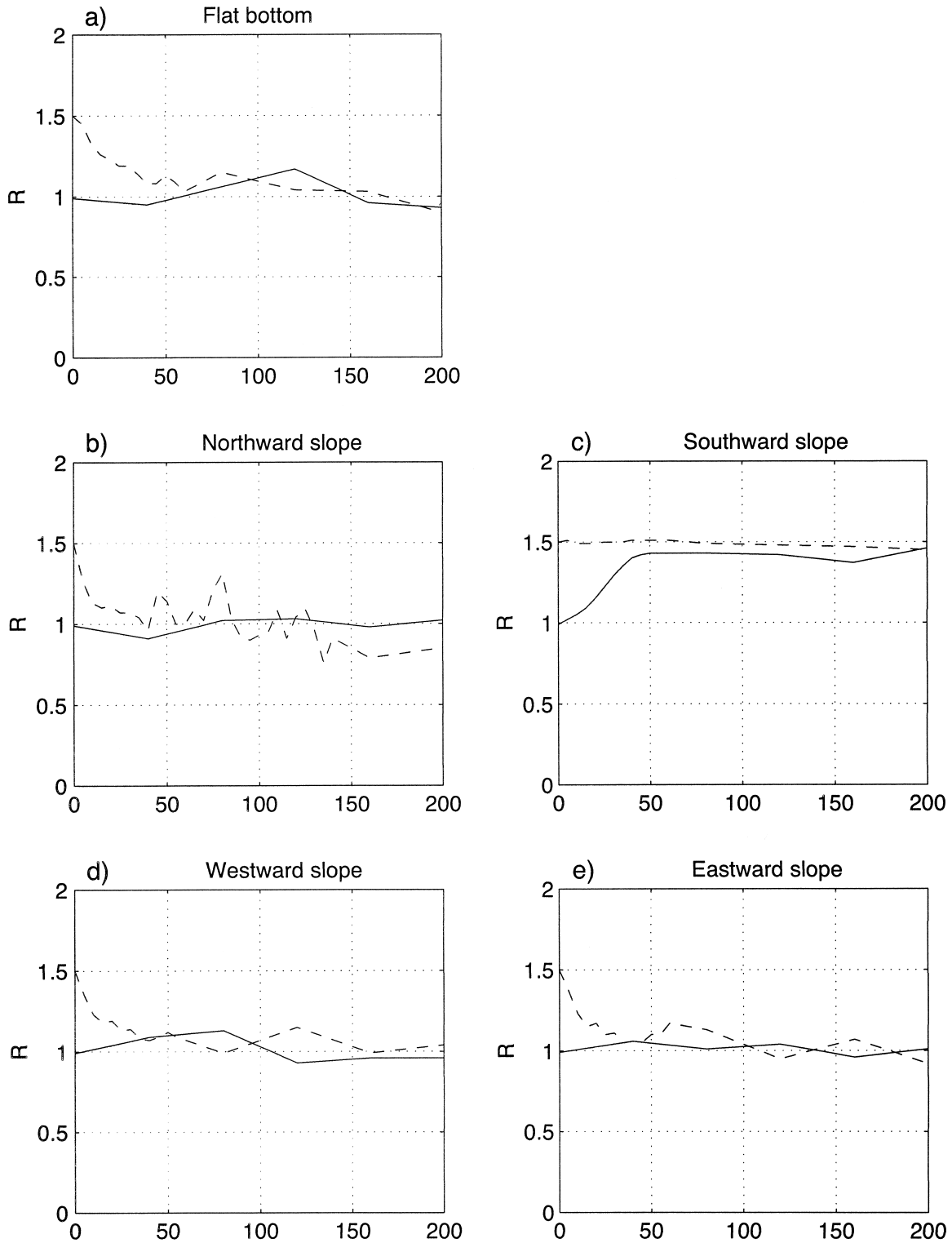
presence of topography was next investigated using the two-layer approximate model proposed by Dewar and Gailliard (1994), modified to include topography. The validity of this simplified model was evaluated by comparing the results with those of a two-layer full primitive equation model—the Miami Isopycnic Coordinate Ocean Model—results that are not limited by a priori simplifications. Remarkably good comparisons were seen for barotropically dominated rings for up to 30 days of evolution in the presence of uniformly sloping topography. To identify the regime of validity of the simple model, numerical experiments were performed

FIG. 17. Time evolution of the parameter R ($=g\eta_o/g'h_o$) for the four topographic orientations and for the B and C series of experiments initialized with $R = 1$ and $R = 1.5$, respectively (see Fig. 16 for the corresponding trajectories).
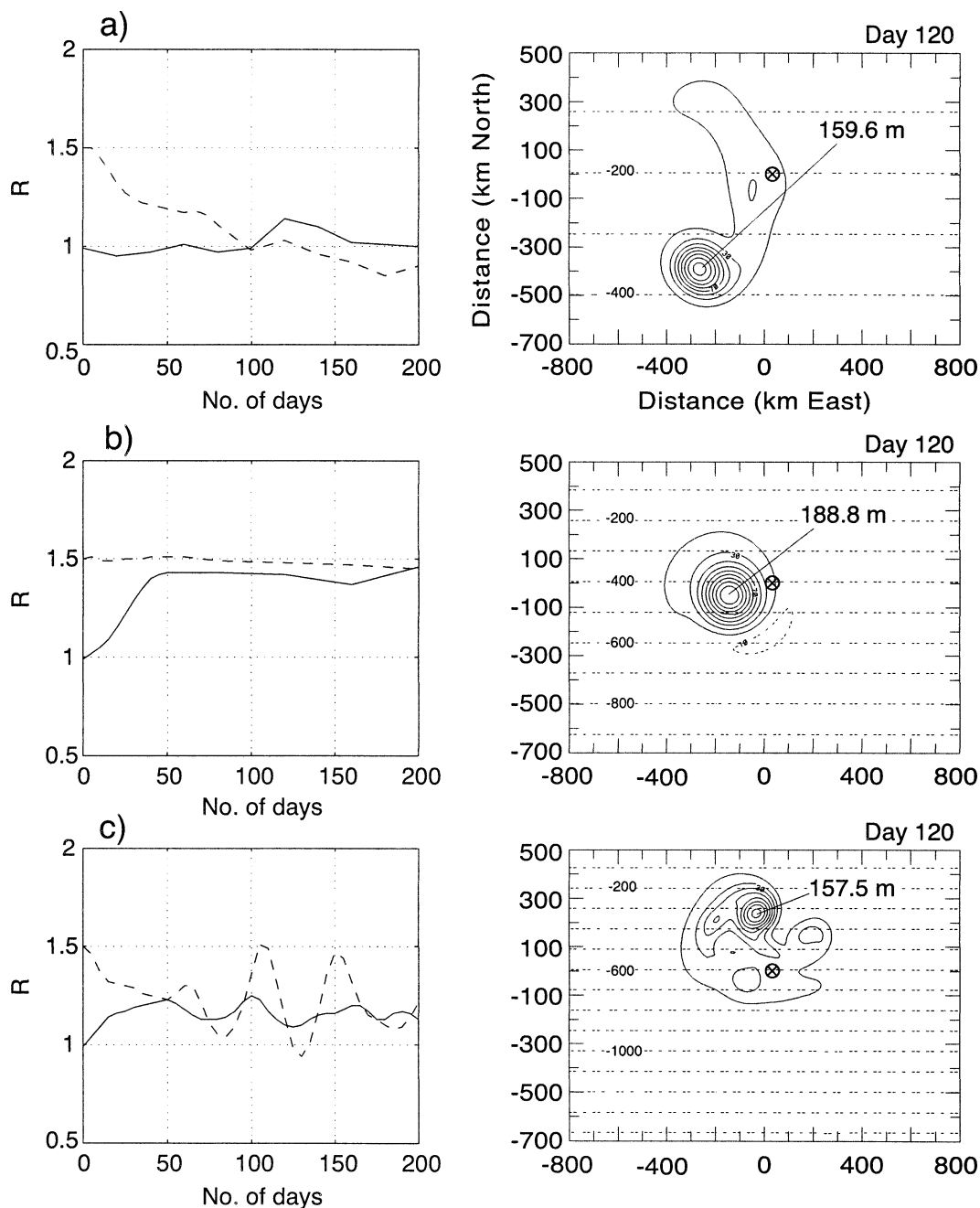
FIG. 18. Time evolution of the parameter R (initially equal to 1 or 1.5) and the interface displacement contour at day 120 for a southward-sloping topography of three different strengths: (a) one-half of the value in B4 and C4, (b) as in B4 and C4, and (c) 2 times the value in B4 and C4. The contour interval is 20 m.

tropic flow, propagating at a very slow rate because of the absence of significant Rossby wave dispersion.

An idealized North Brazil Current ring application was also considered. The simulation produces some results similar to observations (e.g., propagation rate) but fails to produce others because of model shortcomings. Nonetheless, our comparison with analytical expectations is very good, leading us to suggest that sensitivity to deformation radii estimates (extreme in the near-equa-

torial zone) accounts for earlier discrepancies between observations and theory.

REFERENCES

Aagaard, K., and S. A. Malmberg, 1978: Low-frequency character-istics of the Denmark strait overflow. ICES, CM 1978/C:47, 22 pp.

Armi, L., and E. D'Asaro, 1980: Flow structures of the benthic ocean. *J. Geophys. Res.,* **85,** 469–484.

Ball, F. K., 1963: Some general theorems concerning the finite motion of a shallow rotating liquid lying on a paraboloid. *J. Fluid Mech.,* **17,** 240–256.

Bleck, R., and L. T. Smith, 1990: A wind-driven isopycnic coordinate model of the north and equatorial Atlantic Ocean: Model de-velopment and supporting experiments. *J. Geophys. Res.,* **95,** 3273–3285.

——, and E. P. Chassignet, 1994: Simulating the oceanic circulation with isopycnic-coordinate models. *The Oceanus: Physical–Chemical Dynamics and Human Impact,* S. K. Majumdar et al., Eds., The Pennsylvania Academy of Science, 17–39.

Brown, O. B., P. C. Cornillon, S. R. Emmerson, and H. M. Carle, 1986: Gulf Stream warm rings: A statistical study of their be-havior. *Deep-Sea Res.,* **33,** 1459–1473.

Bruce, J. G., 1995: Eddies southwest of Denmark Strait. *Deep-Sea Res.,* **42,** 13–29.

Byrne, A. D., A. L. Gordon, and W. F. Haxby, 1995: Agulhas eddies: A synoptic view using Geosat ERM data. *J. Phys. Oceanogr.,* **25,** 902–917.

Carnevale, G. F., G. K. Vallis, R. Purini, and M. Briscolini, 1988: Propagation of barotropic modons over topography. *Geophys. Astrophys. Fluid Dyn.,* **41,** 45–101.

——, R. C. Kloosterziel, and G. J. F. van Heijst, 1991: Propagation of barotropic vortices over topography on a rotating tank. *J. Fluid Mech.,* **233,** 119–139.

Chassignet, E. P., 1992: Rings in numerical models of ocean general circulation: A statistical study. *J. Geophys. Res.,* **97,** 9479–9492.

——, and B. Cushman-Roisin, 1991: On the influence of a lower layer on the propagation of nonlinear oceanic eddies. *J. Phys. Oceanogr.,* **21,** 939–957.

——, D. B. Olson, and D. B. Boudra, 1990: Motion and evolution of oceanic rings in a numerical model and in observations. *J. Geophys. Res.,* **95,** 22 121–22 140.

Cheney, R. E., and P. L. Richardson, 1976: Observed decay of cy-clonic Gulf Stream rings. *Deep-Sea Res.,* **23,** 143–155.

Clement, A. C., and A. L. Gordon, 1995: Absolute velocity field of Agulhas eddies and the Benguela Current. *J. Geophys. Res.,* **100,** 22 591–22 601.

Cushman-Roisin, B., E. P. Chassignet, and B. Tang, 1990: Westward motion of mesoscale eddies. *J. Phys. Oceanogr.,* **20,** 758–768.

Dewar, W. K., 2002: Convection in small basins. *J. Phys. Oceanogr.,* **32,** 2766–2788.

——, and C. Gailliard, 1994: The dynamics of barotropically dom-inated rings. *J. Phys. Oceanogr.,* **24,** 5–29.

——, and P. D. Killworth, 1995: On the stability of oceanic rings. *J. Phys. Oceanogr.,* **25,** 1467–1487.

Firing, E., and R. C. Beardsley, 1976: The behavior of a barotropic eddy on a β plane. *J. Phys. Oceanogr.,* **6,** 57–65.

Flierl, G. R., 1977: The application of linear quasigeostrophic dy-namics to Gulf Stream rings. *J. Phys. Oceanogr.,* **7,** 365–379.

——, 1984: Rossby wave radiation from a strongly nonlinear warm eddy. *J. Phys. Oceanogr.,* **14,** 47–58.

Fratantoni, D. M., W. E. Johns, and T. L. Townsend, 1995: Rings of the North Brazil Current: Their structure and behavior inferred from observations and a numerical simulation. *J. Geophys. Res.,* **100,** 10 663–10 654.

Grimshaw, R., D. Broutman, X. He, and P. Sun, 1994: Analytical and numerical study of a barotropic eddy on a topographic slope. *J. Phys. Oceanogr.,* **24,** 1587–1607.

Houghton, R. W., R. Schlitz, R. C. Beardsley, B. Butman, and J. C. Chamberlin, 1982: The Middle Atlantic Bight cold pool: Evo-lution of the temperature structure during summer 1979. *J. Phys. Oceanogr.,* **12,** 1019–1029.

Johns, W. E., T. N. Lee, F. A. Schott, R. J. Zantopp, and R. H. Evans, 1990: The North Brazil Current retroflection: Seasonal structure and eddy variability. *J. Geophys. Res.,* **95,** 22 103–22 120.

Kamenkovich, V. M., M. N. Koshlyakov, and A. S. Monin, Eds., 1986: *Synoptic Eddies in the Ocean.* D. Reidel, 433 pp.

——, Y. P. Leonov, D. A. Nechaev, D. A. Byrne, and A. L. Gordon, 1996: On the influence of bottom topography on the Agulhas eddy. *J. Phys. Oceanogr.,* **26,** 892–912.

Killworth, P. D., 1983: On the motion of isolated lenses on a beta-plane. *J. Phys. Oceanogr.,* **13,** 368–376.

Lebel, D., 1994: Topographic effects on the propagation of isolated eddies. WHOI Tech. Rep. 97-18, WHOI Summer GFD Program, 310–334.

McCartney, M. S., and M. E. Woodgate-Jones, 1991: A deep-reaching anticyclonic eddy in the subtropical gyre of the eastern South Atlantic. *Deep-Sea Res.,* **38** (Suppl.), 441–443.

McWilliams, J. C., and G. R. Flierl, 1979: On the evolution of iso-lated, nonlinear vortices. *J. Phys. Oceanogr.,* **9,** 1155–1182.

Mied, R. P., and G. J. Lindemann, 1979: The propagation and evo-lution of cyclonic Gulf Stream rings. *J. Phys. Oceanogr.,* **9,** 1183–1206.

Mory, M., 1985: Integral constraints on bottom and surface isolated eddies. *J. Phys. Oceanogr.,* **15,** 1433–1438.

——, M. E. Stern, and R. W. Griffiths, 1987: Coherent baroclinic eddies on a sloping bottom. *J. Fluid Mech.,* **183,** 45–62.

Nof, D., 1981: On the β-induced movement of isolated baroclinic eddies. *J. Phys. Oceanogr.,* **11,** 1662–1672.

——, 1983a: On the migration of isolated eddies with application to Gulf Stream rings. *J. Mar. Res.,* **41,** 399–425.

——, 1983b: The translation of isolated cold eddies on a sloping bottom. *Deep-Sea Res.,* **30,** 171–182.

——, and T. Pichevin, 1996: The retroflection paradox. *J. Phys. Oceanogr.,* **26,** 2344–2358.

Olson, D. B., 1991: Rings in the ocean. *Annu. Rev. Earth Planet. Sci.,* **19,** 283–311.

——, and R. H. Evans, 1986: Rings of the Agulhas Current. *Deep-Sea Res.,* **33,** 27–42.

——, R. W. Schmitt, M. Kennelly, and T. M. Joyce, 1985: A two layer diagnostic model of the long term physical evolution of warm core ring 82B. *J. Geophys. Res.,* **90,** 8813–8822.

Richardson, P. L., D. Walsh, L. Armi, M. Schroder, and J. F. Price, 1989: Tracking three Meddies with SOFAR floats. *J. Phys. Oceanogr.,* **19,** 371–383.

——, G. E. Hufford, R. Limeburner, and W. S. Brown, 1994: North Brazil Current retroflection eddies. *J. Geophys. Res.,* **99,** 5081–5093.

Schmitt, R. W., and D. B. Olson, 1985: Wintertime convection in warm core rings: Thermocline ventilation and formation of me-soscale lenses. *J. Geophys. Res.,* **90,** 8823–8837.

Shi, C., and D. Nof, 1993: The splitting of eddies along boundaries. *J. Mar. Res.,* **51,** 771–795.

Simmons, H., and D. Nof, 2002: The squeezing of eddies through gaps. *J. Phys. Oceanogr.,* **32,** 314–335.

Smith, D. C., IV, and R. O. Reid, 1982: A numerical study of non-frictional decay of mesoscale eddies. *J. Phys. Oceanogr.,* **12,** 244–255.

——, and J. J. O'Brien, 1983: The interaction of a two layer isolated mesoscale eddy with bottom topography. *J. Phys. Oceanogr.,* **13,** 1681–1697.

Stern, M., 1975: Minimal properties of planetary eddies. *J. Mar. Res.,* **33,** 1–13.

Sutyrin, G. G., 2001: The effects of topography on the β-drift of a baroclinic vortex. *J. Mar. Res.,* **59,** 977–989.

van Ballegooyen, R. C., M. L. Grundlingh, and J. R. R. Lutjeharms, 1994: Eddy fluxes of heat and salt from the southwest Indian Ocean into the southwest Atlantic Ocean: A case study. *J. Geo-phys. Res.,* **99,** 14 053–14 070.

Whitehead, J. A., M. E. Stern, G. R. Flierl, and B. A. Klinger, 1990: Experimental observations of baroclinic eddies on a sloping bot-tom. *J. Geophys. Res.,* **95,** 9585–9610.